Chinese Physics B

TOPICAL REVIEW

One-dimensional sp carbon: Synthesis, properties, and modifications

To cite this article: Chao-Fan Lv *et al* 2022 *Chinese Phys. B* **31** 128103

TOPICAL REVIEW — The third carbon: Carbyne with one-dimensional sp-carbon

One-dimensional sp carbon: Synthesis, properties, and modifications

Chao-Fan Lv(吕超凡)[1,2,3], Xi-Gui Yang(杨西贵)[3,†], and Chong-Xin Shan(单崇新)[3,‡]

[1] *State Key Laboratory of Luminescence and Applications, Changchun Institute of Optics, Fine Mechanics and Physics, Chinese Academy of Sciences, Changchun* 130033, *China*

[2] *University of Chinese Academy of Sciences, Beijing* 100049, *China*

[3] *Henan Key Laboratory of Diamond Optoelectronic Materials and Devices, Key Laboratory of Material Physics, Ministry of Education, School of Physics and Microelectronics, Zhengzhou University, Zhengzhou* 450052, *China*

(Received 15 May 2022; revised manuscript received 1 August 2022; accepted manuscript online 5 August 2022)

Carbyne, as the truly one-dimensional carbon allotrope with sp-hybridization, has attracted significant interest in recent years, showing potential applications in next-generation molecular devices due to its ultimate one-atom thinness. Various excellent properties of carbyne have been predicted, however, free-standing carbyne sample is extremely unstable and the corresponding experimental researches and modifications are under-developed compared to other known carbon allotropes. The synthesis of carbyne has been slowly developed for the past decades. Recently, there have been several breakthroughs in *in-situ* synthesis and measurement of carbyne related materials, as well as the preparation of ultra-long carbon chains toward infinite carbyne. These progresses have aroused widespread discussion in the academic community. In this review, the latest approaches in the synthesis of sp carbon are summarized. We then discuss its extraordinary properties, including mechanical, electronic, magnetic, and optical properties, especially focusing on the regulations of these properties. Finally, we provide a perspective on the development of carbyne.

Keywords: carbyne, polyyne, linear carbon chains

PACS: 81.07.Gf, 73.90.+f, 78.67.Uh, 63.22.Gh **DOI:** 10.1088/1674-1056/ac872f

1. Introduction

With different orbital hybridizations and flexible bonding ways, numerous kinds of allotropes have been discovered in carbon. Diamond consists of sp^3-hybridized carbon atoms, whereas sp^2 hybridization is present in graphite, graphene, fullerene and carbon nanotube. Each of them shows unique mechanical, electronic, and optical properties. For instance, diamond is the hardest material ever known and wide gap semiconductor with an indirect bandgap of 5.36 eV. In contrast, graphene has the characteristic semimetal electronic structure with an ultra-high electron mobility.

Different from graphene and diamond, as shown in Fig. 1, carbyne is a one-dimensional carbon allotrope formed by straight lines of sp-hybridized carbon atoms with infinite length.

As shown in Fig. 2(a), two possible forms of carbyne are further distinguished based on the chemical bond structure: the term polyyne follows Peierls distortion theory,[2] has been used to describe a bond length alternated structure, characterized by alternating conjugated single and triple bonds (BLA$\neq$ 0); on the other hand, β-phase or "cumulene" denotes an infinite chain, characterized by all-equal double bonds (BLA = 0).[3]

Band structure and potential energy analysis are shown for the cumulene and polyyne (Figs. 2(b) and 2(c)). It is shown that the cumulene with equidistant C=C bond has two degenerate half-filled p-bands; the polyyne with alternating CC and C≡C bonds has fully filled band, owing to two electrons provided to each orbital and a half Brillouin zone, and the band is separated by the band gap leading to semi-conductivity. The linear connection of bond length alternation (BLA) and electronic properties (band gap) has been well summarized previously and shown in Fig. 3.

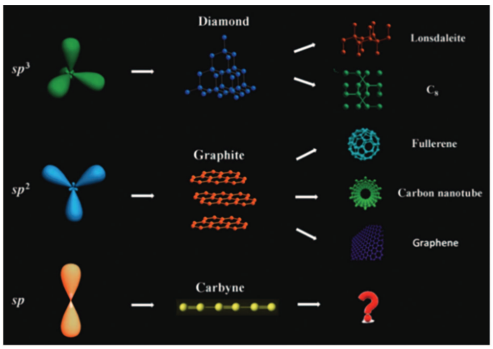

Fig. 1. Schematic illustration of the three kinds of hybridization of carbon. Diamond represents sp^3 hybridization and its derivatives are lonsdaleite and C_8. The most familiar carbon material, graphite, shows sp^2 hybridization, and its derivatives are fullerene, carbon nanotube, and graphene. Carbyne is the one-dimensional allotrope of carbon composed of sp-hybridized carbon atoms. Reprinted with permission,[1] copyright ©2015 American Association for the Advancement of Science. All rights reserved.

†Corresponding author. E-mail: yangxg@zzu.edu.cn

‡Corresponding author. E-mail: cxshan@zzu.edu.cn

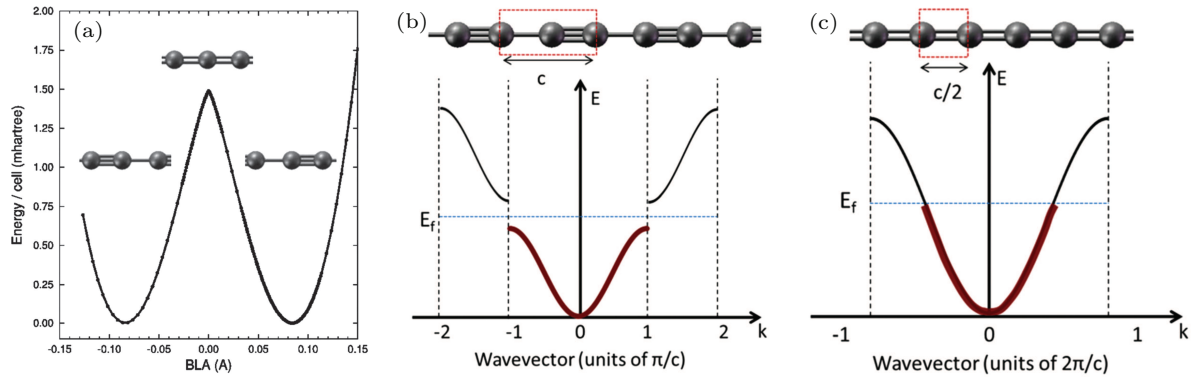

Fig. 2. (a) Potential energy surface of an isolated infinite linear carbon chain as a function of BLA, showing the occurrence of Peierls distortion (instability of the equalized, cumulene-like geometry) and the stabilization of the two possible (and equivalent) bond alternated (polyyne-like) structures. (b)–(c) Sketch of the two polyyne and cumulene, band filling reveals the metal and semiconducting character of cumulene and polyyne, respectively. Reprinted with permission,[4] copyright ©2016 ©The Royal Society of Chemistry. All rights reserved.

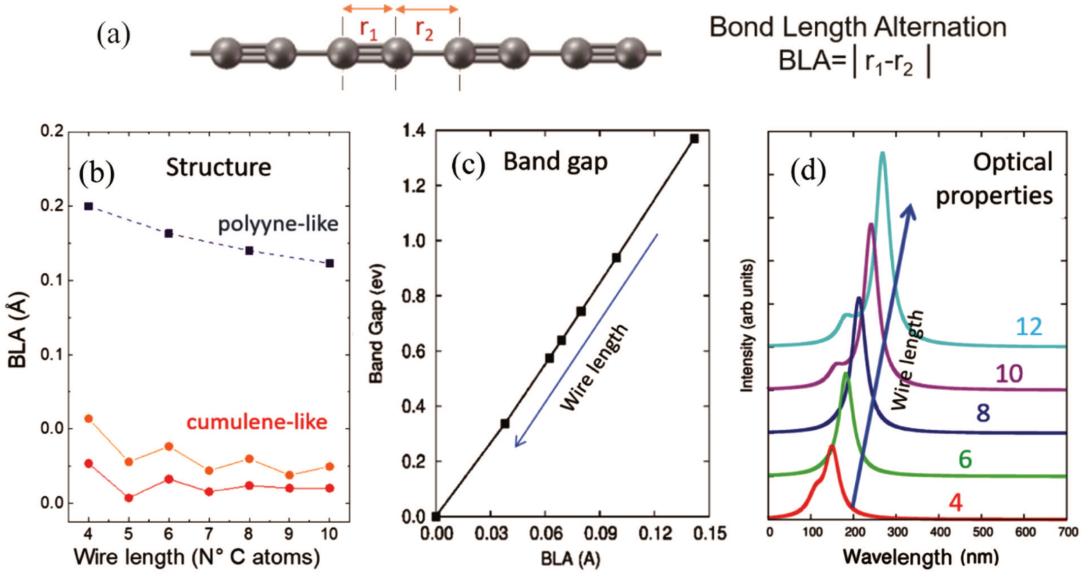

Fig. 3. (a) BLA as the parameter to describe the structure of carbyne. (b) DFT computed BLA values for polyynic and cumulenic structure (the red line refers to uncapped Cn chains, the orange one to vinylidene-capped chains). (c) Evolution of the band gap for finite polyynes for increasing length. (d) Calculated optical spectra for H-terminated polyynes with length ranging from 4 to 12 carbon atoms. Reprinted with permission,[5] copyright ©2018 ©Materials Research Society. All rights reserved.

Due to the Peiers distortion theory in one-dimensional (1D) system, the stable form is polyyne for an infinite carbyne (Fig. 2(c)).[4] The *ab-initio* calculations also indicated that polyyne has a better thermodynamic stability than cumulene,[6] calculations based on the density functional theory (DFT) regarded cumulene as a transition state of carbon chain in a thermodynamically structural evolutional process.[7] Experimental consequence also confirmed these judgments: the polyyne is superior than cumulene both on the air stability and the length of the experimentally synthesized sample currently.[8–11]

Theoretical predictions pointed out exceptional properties of infinite carbyne in mechanical, electromagnetic and optoelectronic field, making carbyne a promising champion material. However, only finite polyyne (few cumulene) can be experimentally synthesized in the laboratory.

Hampered with the inherent instability of sp-hybridized bonds and relatively soften one dimensional structure, the free-standing carbyne possess high chemical reactivity and tends to undergo chains cross-linking reaction and transformation of sp^2 solid phase.[12] There are three methods that are mainly used to overcome these limits to date: the en-dcap group's introducing (Figs. 4(a) and 4(b)), crystallization with Van der Waals interaction between parallel chains (Fig. 4(c)) and linear carbon chains encapsulated with CNTs (LCC@CNTs) (Fig. 4(d)). since various names have been used in the literatures for these synthesized carbon chains, in the review, we simply named these different samples polyyne/endcapped polyyne, carbyne crystals and LCC@CNTs separately.

Currently, the longest free standing polyyne containing 48 contiguous acetylenic carbon atoms synthesized via end-capping organic group was realized by Gao and Chalifoux in 202.[9] Remarkably, LCC more than 100 carbon atoms have been grown inside multiwalled carbon nanotubes (MWC-

NTs) by arc-discharge method in 2003,[13] which shed light on the possibility toward infinite carbyne by using CNT as a nano template for the synthesis and preservation of LCC. In 2016, Shi *et al*. established a route for synthesis of extremely long and stable LCC containing more than 6000 carbon atoms encapsulated into double-walled carbon nanotubes (DWCNTs).[14] Short carbon chains have also been observed when pulling the graphene or CNT before breaking.[15] The formation of carbyne crystals by laser ablation in liquids have been proposed by Pan *et al*.[1] However, the claiming of bulk carbyne crystals also stimulated criticism and discussion, further work is needed to shed light on bulk carbyne, which is a still open and interesting research topic.[5,16]

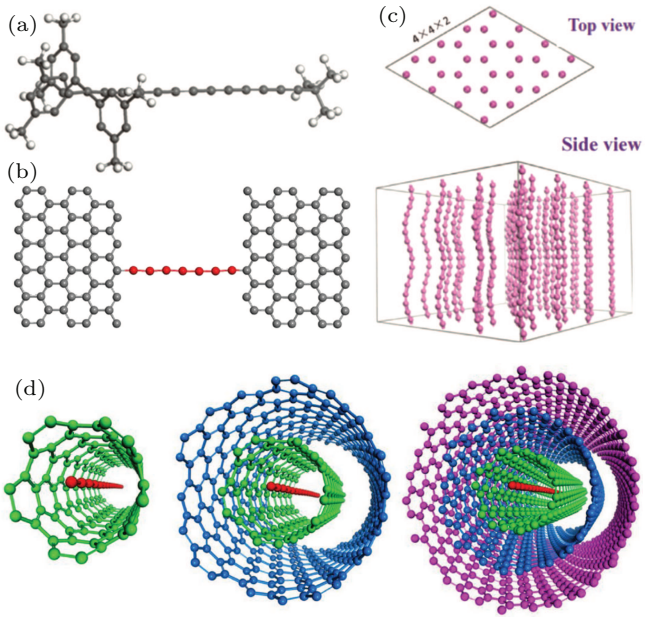

Fig. 4. (a)–(b) End-capped polyynes. (c) The scheme of crystalline carbyne. (d) LCCs inside SWCNT, DWCNTs, and MWCNT. Reprinted with permission,[12] copyright ©2020 Chinese Chemical Society and Institute of Materia Medica, Chinese Academy of Medical Sciences. Published by Elsevier B.V. All rights reserved.

Parallel to the exploitation of different synthesis method of carbyne, great progress of investigation and interpretation of the relationship between chains length, BLA value and mechanical/optoelectronic properties have been made.[4,5] It was also found various external field and strains would modulation physical properties (conductance, lowest unoccupied molecular orbital–highest occupied molecular orbital (LUMO–HOMO) band gap, vibration, and even magnetism) of carbyne by altering BLA value.

In this review, we will mainly focus on introducing carbyne from different forms of experimental existence and its physical properties under different external field. The investigations on the theoretical predicted and experimentally observed physical properties of carbyne will be introduced firstly, and then experimental results mainly on synthesis of polyyne and LCC@CNT will be discussed. Finally, variations in the physical properties of carbyne under different external conditions will also be presented briefly. Perspectives are discussed in several sections and in the summary.

2. Synthesis of one-dimensional sp carbon

Due to the inherently unstable nature of sp hybridization, polyynic carbon chains can be decomposed easily when exposure to oxygen and/or water surroundings,[17] and possessed high reactivity to undergo chains cross-linking reaction and formed sp^2 solid phase,[18] as indicated by previous studies on isolated carbon chains in gas phase[19,20] or at very low temperature.[21]

Currently, the main route to protect the polyyne is end-capping with organic group and sp^2 graphene or encapsulating inside CNTs. Based on these principles, different methods have been proposed to synthesis carbon chains toward carbyne. A brief introduction will be present in the following subsections.

2.1. Bottom-up synthesis of end-capped Polyyne

The bottom-up organic chemical reactions synthesis method of polyyne was carried by Baeyer in 1885 first,[22] in which short polyynic chains reacted with each other and eventually form longer chains with length of 8 carbon atoms. This method has been sufficiently developed by inducing terminal groups to stabilize the chain, in which the terminal group can be a simple hydrogen atom or large organic group whose molecular weight may even exceeds carbon chain skeleton, eventually represent a dumbbell structure. Various of heteroatom end-capped polyynes, such as hydrogen,[23–25] alkyl,[26–28] aryl,[29] trialkylsilyl,[9] and metal.[30–35] In 2020, Gao and Chalifoux *et al*. reported the synthesis of longest free standing polyyne end-capped by trismethyl with up to 48 carbon atoms.[9] This length record was held till this day.

Initially, the synthesis of polyyne belonged to the realm of organic chemistry and was achieved in by a complex, impressive and elegant synthetic procedure. Subsequent a relatively simple and economic set up was induced to synthesize carbon chains: two graphite electrodes submerged in an organic solvent and connected to a DC power supply, named as arc discharge method. Franco Cataldo *et al*. showed that polyynes mixture can be easily synthesized in one shot and with relatively bulk quantities when an electric arc was struck between two graphite electrodes submerged in a solvent like methanol, acetonitrile or n-hexane.[36–38] The synthesized carbon-chain with terminal group is usually at a length of 6–24 carbon atoms.

Cataldo *et al*. compared the influence of different precursor solutions and temperatures. It was found that the longest polyyne with 18 carbon atoms was produced when

acetonitrile was arced at 40 °C, instead, at room temperature the entire polyynes produced was less than 16 carbon atoms. Subsequently, researchers extended electrode materials and solutions to synthesis polyyne through similar arc discharge configuration, such as graphite electrodes in liquid nitrogen,[39] nickel electrodes in alcohol,[40] copper electrodes in alkanes,[41] and graphite electrodes in pure water.[42,43]

Similar with the arc discharge method, when the graphite target is placed in organic solution, a focused pulsed laser would generate a high temperature thermal field on the target to produce polyyne.[44–46]

Tsuji *et al*. found that Polyynic molecule $C_{16}H_2$ can be obtained by laser ablation of graphite powders suspended in benzene, toluene, and hexane solutions.[45] The obtained polyynes had different lengths and different terminations, depending on the precursor and solvent used.

A well-supported hypothesis suggested the growth process of polyyne is carried out by continuous coupling of C_1 and C_2 radicals. This process competed with the termination mechanism due to the formation of chemical bonds between carbon radicals and end group radicals, usually hydrogen in these organic solutions.[45] The longest polyyne detected after pulse laser ablation synthesis was with 30 carbon atoms, obtained by Matsutani and co-workers ablating a graphite rod in decalin.[47]

2.2. Synthesis of carbyne crystals

It's worth noting that with the presence of Au nano particles, the radiation of focused pulsed laser on carbon source target will produce carbyne crystals formed by Van der Waals interaction between parallel polyynic chains. Pan *et al*. reported the synthesis of carbyne crystals firstly, which are separated from ns pulse laser ablated gold target immersed in alcohol solution. Pan and coworker believed the peaks around 1050 cm^{-1} and 2175 cm^{-1} found in the Raman and FTIR spectrum was originated from the single and triple bond in polyynic chains (Figs. 5(c) and 5(d)), respectively.

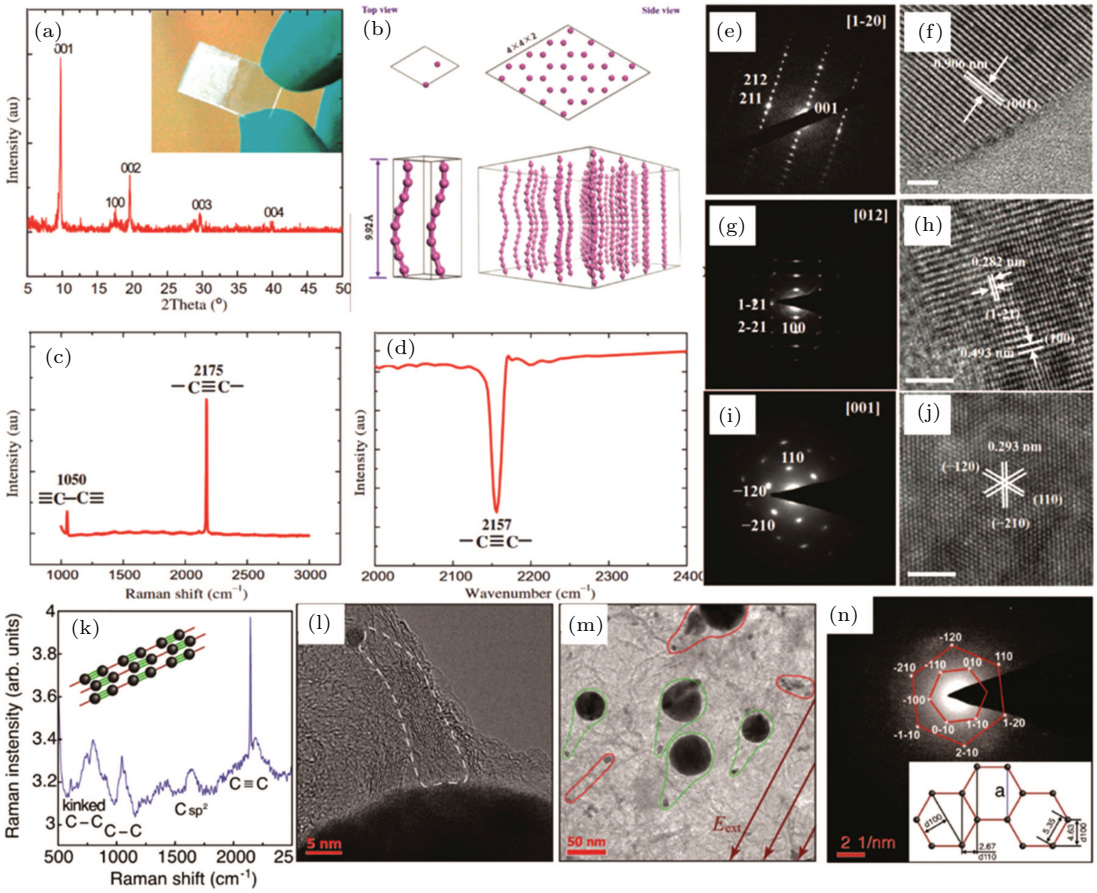

Fig. 5. Morphology and structural characterization of carbyne crystals synthesized by laser ablation. (a) XRD pattern of the sample. Inset: White carbyne powder coating on the glass substrate. (b) The equilibrium configuration of the constructed carbyne crystals based on first-principles calculations. They are in the shape of flakes stacked together. (c)–(d) Raman and FTIR spectrum. The Raman peaks at 1050 cm^{-1} and 2175 cm^{-1} belong to carbon–carbon single bonds and triple bonds, respectively, the signal at 2157 cm^{-1} in FTIR spectrum is ascribed to the stretching vibration of carbon–carbon triple bonds. (e)–(j) TEM image and corresponding selected area electron diffraction (SAED) patterns of carbyne crystals, divided into three categories based on the direction of the incident electron beam ([1-20], [012], and [001]. Reprinted with permission,[1] copyright ©2015 American Association for the Advancement of Science. All rights reserved. (k) The Raman spectrum. (l) TEM image of the carbyne wire bundles attached to two NP, at the bottom corresponds to the larger NP of a nearly spherical shape with the radius ∼ 25 nm. (m) An ensemble of closely spaced nano-dipoles oriented along the electric field direction (marked by green curves). The randomly oriented carbyne complexes without gold NPs framed with red curve demonstrate no sensitivity to the electric field. (n) The SAED of a thin deposited layer. The reflexes are labeled with the corresponding Miller indices. The insert shows the corresponding real-space structure of a carbyne crystals in the direction perpendicular to the chains. The parallel chains are hold together by the van der Waals interaction. Reprinted with permission,[50] copyright ©2020, The Author(s). All rights reserved.

Besides, the hexagonal crystalline structure of these carbyne crystals was confirmed with XRD and selected area electron diffraction (SAED) patterns and high-resolution transmission electron microscope (HRTEM) images in Fig. 7(a) and Figs. 5(e) and 5(f). The parallel polyynic chains are not straight but kink along the *c* axis.[1] This work also leaded to the consolidation of the ends of linear chains on the surface of gold nanoparticles and prevents their further curling into coils.

Later, this stabilized carbyne crystals polyyne-metal nano particle complexes by laser ablation of colloidal carbon systems were prepared by pulse laser ablation.[48,49] Furthermore, Kutrovskaya *et al*. demonstrated a new efficient approach to the substrate deposition of agminated polyynic wires which enables for the spatial ordering of multiple chains stabilized by gold nano particles (Fig. 5(m)).[50] In this method, Kutrovskaya and coworkers took advantage of the dipole moment created by two gold nano particals (NPs) with different size and work functions at the opposite ends of chains, introduced an external electric field for the ordering of parallel polyynic chains end capped with gold nano particles. Similar with the reporting from Pan *et al*. the agminated polyynic wires presented hexagonal phase and two sharp Raman peaks as shown in Fig. 5(k).

2.3. Synthesis of LCC@CNTs

As a nano template for the molecules' aggregation and chemical reaction, the one-dimensional hollow structure of CNTs provide ideal environments for the creation of isolating individual atomic chain.[51–57] Currently, carbyne consisting of more than 50 carbon atoms can only be synthesized inside carbon nanotubes.

In 2003, Zhao *et al*. first obtained LCC@MWCNTs comprising $\approx$ 100 carbon atoms which deposited on the surface of pure carbon cathode by the DC arc discharge evaporation in hydrogen gas.[13] Raman spectra of the materials show characteristic C-band between 1820 cm^{-1} and 1860 cm^{-1}, attributed to the impanel stretch vibration mode of the chains inside CNTs. Initially, Raman spectroscopy and side section TEM images were used as experimental evidence for the successful synthesis of LLCC@MWCNTs.[58] In 2015, Andrade *et al*. took a clear images though cross section of individual chain inside CNT by scanning transmission electron microscopy (STEM), which demonstrated the existence of carbon atom chains within the innermost CNT unambiguously.[59]

In addition, LCC@MWCNTs were also synthesized in hydrogen, argon and helium gas by arc dis charge method. Aimed at the purpose of large-scale and high purity preparation, Kim *et al*. developed an arc apparatus to continually produce MWCNT tapes by atmospheric arc discharge.[60] Nevertheless, by introducing a cooling system[61] and static magnetic field[62] into the conventional hydrogen arc discharge equipment, Zhang *et al*. have improved both the growth yield and purity of the final product.

HR-TEM images of adamantane molecules encapsulated in DWCNTs with inner diameter (b) $d < 0.8$ nm (no encapsulation), (c) $d \approx 1.0$ nm (single linear array of adamantane molecules), (d) $d \approx 1.4$ nm (double array of adamantane molecules), (e) $d \approx 1.8$ nm (multiple arrays of adamantane molecules). Reprinted with permission,[63] copyright ©2012 American Chemical Society. All rights reserved.

The aggregation and reaction of organic molecular inside CNTs was also carried out to grow LCC inside CNTs after the observation LCC@MWCNT. The first observation was reported by Nishide, in which polyynic molecules $C_{10}H_2$ were encapsulated by SWNTs.[64] Zhang *et al*. reported the assembly and thermal transformation of LCC@DWCNTs by vacuum annealing (1500 K, 48 hours) of adamantane molecules encapsulated in a carbon nanotube, the schematic diagram and TEM image of LCC@DWCNTs were shown in Fig. 6, the TEM image confirmed the appropriate diameter of CNT was $\sim$ 1.1 nm to synthesize linear carbon chain inside CNT.[63] Deng *et al*. studied the affecting factors of carbyne synthesis, investigating the effects of temperature, confinement (via nanotube diameter) and alignment (using polymer shape metrics) systematically, delineated the optimal conditions for LCC's growth inside SWCNTs.[65]

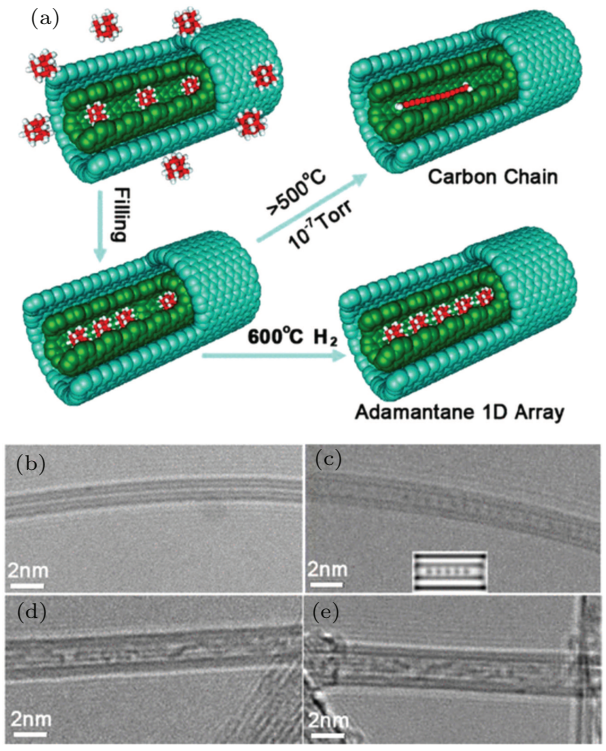

Fig. 6. (a) Schematic diagram of synthesis and annealing of linear adamantane assemblies.

Except for filling the precursor molecular into the CNT before heating, the carbon atoms remaining on the CNT walls can also be used as the carbon source to synthesize LCC. Endo

et al. first proved that anneal the CNTs at 1600 K directly could produce LCC, however, Endo *et al*. believed that the carbon chains were grown between neighbor DWCNTs but not inside the inner tubes of the DWCNTs.[66] After High temperature heat treatment at $\sim$ 1900 K, Jinno *et al*. observed the characteristic C-band Raman peak at $\sim$ 1855 cm^{-1} in the MWCNTs and DWCNTs with the innermost tube diameter of $\sim$ 0.6 nm,[67] which match well with the wrapped structure of LCC@MWCNT previously reported in arc discharge methds.[13]

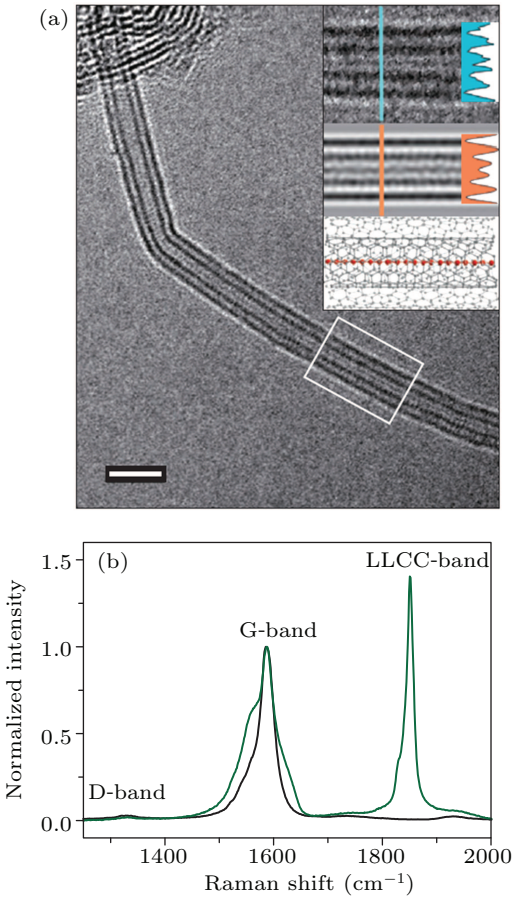

Fig. 7. (a) HRTEM image of an LCC@DWCNT. Inset: an enlarged part of the HRTEM image (top), a simulated HRTEM of an LLCC@DWCNT (middle), and a molecular model of an LLCC@DWCNT (bottom). The corresponding line profiles of the experimental and a simulated LCC@DWCNT are shown, respectively. (b) Raman spectra of LCCs@DWCNTs carried out at an resonant excitation wavelength of 568.2 nm. D-band, G-band, and C-band (green line) of a sample annealed at 1460 as compared to pristine DWCNTs (black line). Reprinted with permission,[14] copyright ©2016 Macmillan Publishers Limited. All rights reserved.

The formation mechanism is well discussed and compared to the arc discharge method, Sheng *et al*. reported the fabrication of LCC@MWCNTs by a high-temperature treatment of MWCNTs with the innermost tube diameters of $\sim$ 0.7 nm,[68] Shi *et al*. confirmed that LCC can be grown inside the ultrathin DWCNTs with inner diameter of 0.6 nm–1.0 nm by high-temperature treatment. It is suggested the diameter of inner CNT is the crucial condition for the growth of carbon chains. On this basis, Shi *et al*. used the DWCNTs with inner tube diameters between 0.62 nm–0.85 nm as nanoreactors and as shells to encapsulate and protect LCCs. resulting in ultra-long LCCs consisting of more than 6000 carbon atoms directly observed by Tip-enhanced Raman scattering (TERS) mapping, which keeps the world's length record till today, the HRTEM image and Raman spectrum were shown in Fig. 7.[14]

Aimed to the large-scale synthesis of LCC@CNTs by high-temperature annealing method, annealing conditions both vacuum and in inert gas have been approved to yield of linear chains.[66,69] Li *et al*. synthesized LCC@DWCNTs by controlling the gas pressure during the annealing, and found that the yield of the LCCs at applied pressures at 10^1 Pa is good enough for the synthesis, which would practically benefit the future large-scale synthesis and applications of the LCCs.[70]

Although great progress has been made on arc discharge and thermal annealing methods to synthesize LCC@CNTs, it is important to keep in mind that these methods can only be applied to bulk samples. This represents a drawback if we look at the possibility to carry out the synthesis in single CNT with special chirality. A perfect alternative to perform the synthesis in such case is a localized photothermal heating by means of laser annealing, which has been used to change the structure of CNT related materials previously.[71,72]

Ha *et al*. first demonstrated the coalescence behavior between SWNTs and the formation of LCC femtosecond laser irradiated SWNTs film. The observed Raman frequencies correspond to linear chains $\geq$ 36 atoms.[73] Very recently, Shi *et al*. reported the photothermal growth and *in-situ* Raman characteristic of the carbon chains inside suspended DWCNTs by laser annealing.[74] Compared to the previously furnace-based annealing method, photothermal growth realized by laser annealing opens the possibility to confine carbyne to individualized, aligned, patterned, suspended, substrate-supported, or metallicity/chirality-separated CNTs, on which other special physical properties could be investigated.

2.4. Synthesis of polyyne on metal surface

Surface chemistry is also a promising method for the preparation of various carbon nanostructures, a series of carbon nanostructures have been successfully prepared.[75–77] In 2016, Sun *et al*. reported a successful onsurface synthesis of metalated polyyne by dehydrogenative coupling of ethyne molecules and copper atoms on a Cu (110) surface under 450 K and ultrahigh-vacuum conditions, scanning tunneling microscopy (STM) images in Fig. 8(a) indicated that the carbon chains are arranged along the [1$\bar{1}$0] direction of Cu.[78] Rabia *et al*. synthesized polyyne connected through phenyl groups by on-surface reaction to release bromine atoms in halogenated precursors evaporated on Au (111). The formation and arrangement morphology were confirmed by Raman and STM images.[79]

Recently, Kaiser *et al*. successfully prepared a circular carbon atom chain C_{18} by manipulating a $C_{24}O_6$ as initio reactant on bilayer NaCl on Cu (111) at 5 K via designing a reaction scheme. The reaction pathway and *in-situ* STM image were depicted in Fig. 9, and the obtained circular chain was named as cyclo carbon.[80] These results demonstrated that the strained polyynic moieties of cyclo carbon and its oxide intermediates allowed covalent coupling by atom manipulation, provided a direct experimental insight into the structure of a cyclo carbon and opened the way to create other elusive carbon-rich molecules by atom manipulation.

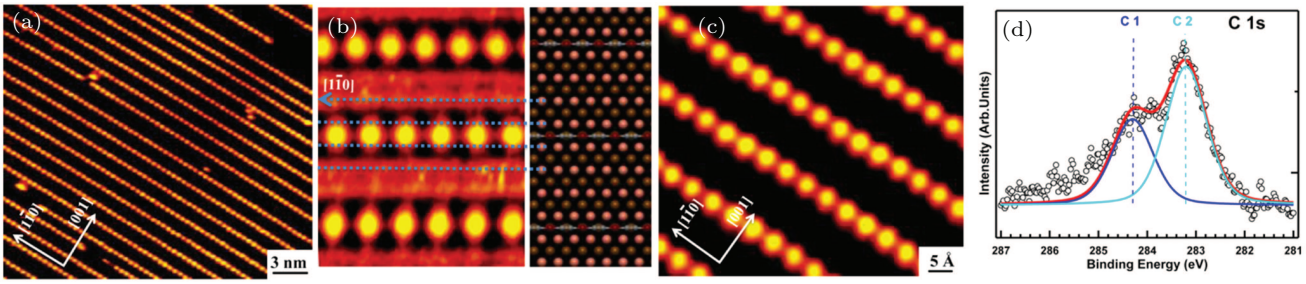

Fig. 8. (a) Large-scale and (b) close-up STM images showing the formation of metalated polyynic chains. (c) High-resolution STM image resolving the metalated polyyne and the substrate lattice simultaneously. The underlying copper rows along the [1$\bar{1}$0] direction are indicated by blue dashed lines. The corresponding DFT-optimized structure model of metalated carbyne is presented aside for comparison. (d) C 1s core-level x-Ray photoelectron spectrum showing the major peak C2 located at a binding energy of 283.2 eV (cyan curve). Reprinted with permission,[78] copyright ©2016 American Chemical Society. All rights reserved.

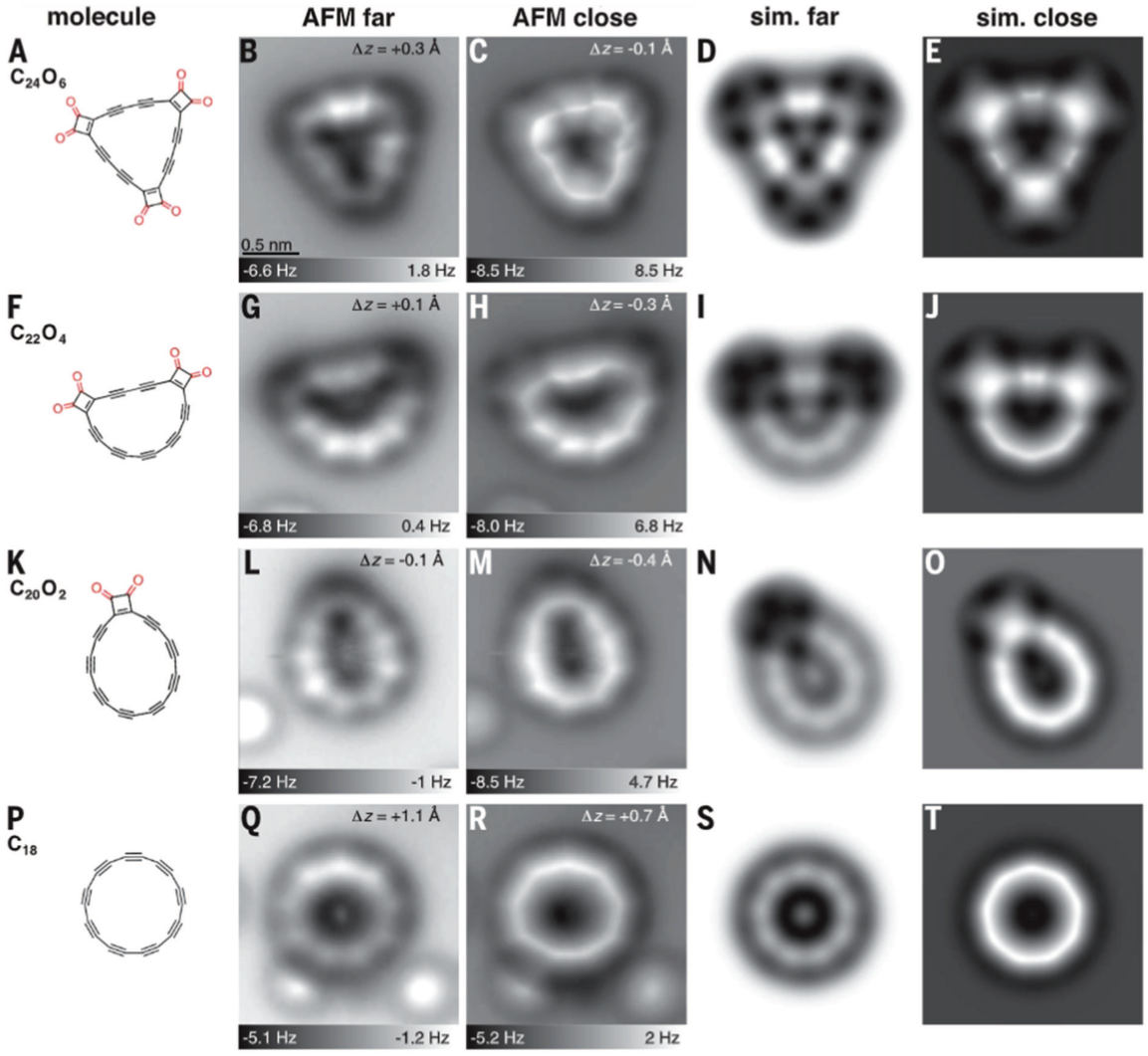

Fig. 9. Precursor and products generated by tip-induced decarbonylation. Structures are shown in column 1. AFM images (columns 2 and 3) were recorded with a CO-functionalized tip at different tip offsets, bright features at each side of the molecule were assigned to triple bonds. (A)–(E) Precursor, (F)–(J) and (K)–(O) intermediates, (P)–(T) cyclo carbon. Columns 4 and 5 show simulated AFM images based on gas-phase DFT-calculated geometries. The difference in probe height between "sim. far" and "sim. close" corresponds to the respective difference between "AFM far" and "AFM close." The scale bar in (B) applies to all experimental and simulated AFM images. Reprinted with permission,[80] copyright ©2019 American Association for the Advancement of Science. All rights reserved.

2.5. *In-situ* synthesis of short carbon chains

Focused electronic beam in TEM was used to "knock out" certain atoms from the original lattice to form specific structure.[81–84] Using this method, Jin *et al*. reported that single atom carbon chains were fabricated by removing carbon atoms row by row from graphene through the controlled energetic electron irradiation. The formation progress of carbon single atom chain was recorded in Fig. 10.[15] Moreover, direct observation of the BLA and carbon chain produced from few layer graphene flakes was presented by Casillas *et al*. using aberration corrected TEM.[85]

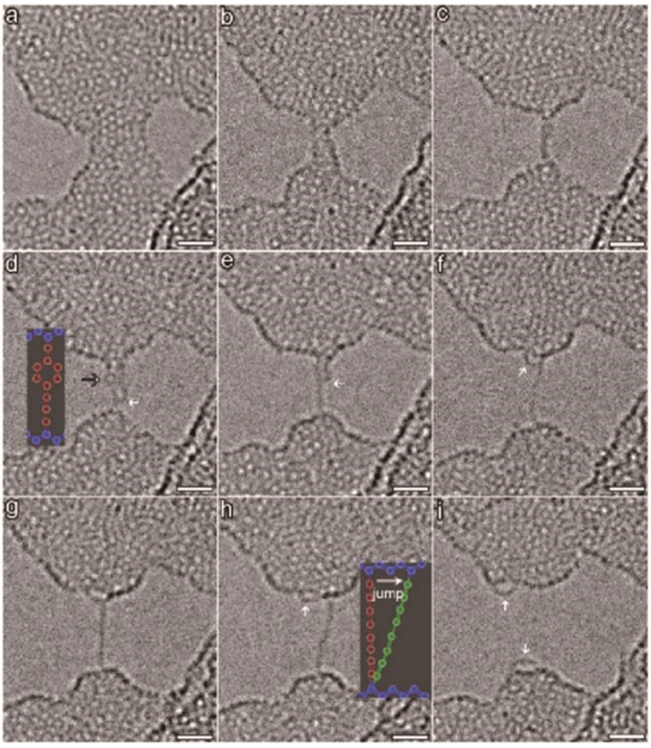

Fig. 10. Consecutive HR-TEM images showing the dynamics for the formation, breakage of freestanding carbon atomic chains through continuous electron beam irradiation. (a) A graphene nano ribbon (GNR) with a width of about 1.7 nm was formed between two holes on the graphene. (b) The GNR was thinned row-byrow under the continuous irradiation. (c) A carbon chain consisting of double strands was formed, and there was a knot remained on the left chain (marked as the black arrow). Inset is a representative scheme. The right chain broke from its bottom end (marked as white arrow) and detached with the graphene edge. (d)–(f) The broken chain (on the right) migrated along the left chain, and finally made a connection with the edge belonging to the upper graphene. (g) The carbon was found to be linear and flexible. (h) The carbon chain made a jump along the graphene edge with a changing of edge bonding. The inset is a representative scheme. (i) The carbon chain broken from its upper head. Again it was able to migrate along the graphene edge. Scale bar, 1 nm. Reprinted with permission,[15] copyright ©2009 American Chemical Society. All rights reserved.

There is a similar method to prepare carbon chains from graphene not by "knock out" but "extract out" with STM tips (Fig. 11), meanwhile, both the synthesis and the electrical characterization of free-hanging atomic carbon chains were carried out *in-situ*. This method was first demonstrated in graphene in 2013.[86] After that, the experimental methods are discussed in detail, with emphasis on the contact between carbon chains and metal tips by La Torre.[85] The *in-situ* measurement of electrical conductivity under tensile stress is realized subsequently.[87]

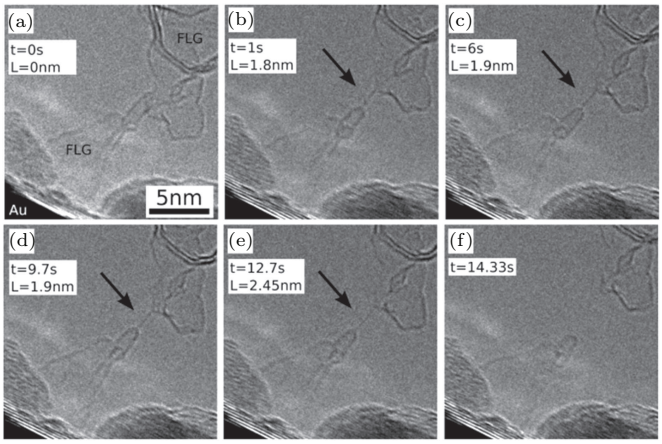

Fig. 11. *In-situ* extract out of a monatomic carbon chain with STM tip in graphene. (a) A few-layer GNR breaks and forms a carbon chain (arrowed) which is stable for a few seconds [(b)–(e)]. The chain eventually breaks and disconnects the two GNR regions (f). The time scale as well as the measured length of the chain (in the projection onto the image plane) are indicated. Reprinted with permission,[86] copyright ©2013 American Chemical Society. All rights reserved.

In general, it is difficult to achieve sufficient length for single atom polyynic chains prepared though bottom-up chemical reaction, laser irradiation, and arc-discharge method, and there are usually complex end-groups introduced to stabilize the chains, which have a great influence on the physical properties of the chains itself. Using the CNTs as a template, extremely long polyynic chains considered as carbyne were synthesized, however, the charge transfer process between the CNTs and the chains also affects the electronic properties of the chains. In addition, short polyynic chains can be prepared on metal surfaces with surface chemistry method, which show certain advantages in characterization and separation.

3. Physical properties of carbyne

In the infinite carbyne, due to the indirect connection to other poly-conjugated molecules, it is obligatory for the present of end group or CNT to stabilize chains and prevent them from cross-linking reaction. Under this situation, it is hard to perform experimental studies of ideal carbyne. Therefore, several theoretical/computational works focused on the simulation of such interesting system, investigated its mechanical and optoelectrical properties. *In-situ* conductance and spectrum experimental tests for some end-capped polyyne, carbyne crystals, LCC@CNTs and short linear carbon chains have also been implemented.

3.1. Mechanical strength

The mechanical properties of carbyne are essential to their successful incorporation in the design of novel devices. Contrary to intuitive impression, carbyne as one-dimensional

chain possesses excellent mechanical property under tensile strain, it is even suggested that carbyne may be the strongest material ever known, including CNT, graphene and diamond.[88]

Ab-initio calculations were performed on polyyne to give numerical results for elastic modulus. The first mechanical properties simulation of polyyne was obtained in 2011, Nair and co-workers identified a length-dependent strength up to 11 GPa, and a peak Young's modulus of 288 GPa. Simultaneously, Zhang and Yang compared Young's modulus of polyyne and cumulene of infinite length and obtained higher value of 1.304 TPa and 760.78 GPa, respectively.[89] For the cumulene configuration Young's modulus are significantly higher than those of polyynes reported from Chang and Zhang,[90,91] while both are comparable to those of the hardest natural materials.

After that, Liu *et al*. found carbyne has an unrivaled specific strength of up to 7.5×10^7 N·m/kg under axial tension, requiring a force of ~ 10 nN to break a single atomic chain, which means carbyne is about twice as stiff as the CNTs ever reported.[92,93]

Besides the free standing polyynic chains, LCC@CNT also provides better mechanical properties in which CNT act as reinforcing building blocks, Gao *et al*. developed a mechanics model for exploring the mechanical properties of multiple LCCs enclasped in single wall carbon nanotube (LCC@SWCNT). Under the premise that carbyne has a higher predicted gravimetric modulus and gravimetric strength than any other form of carbon allotropes. The highest calculated gravimetric modulus and strength were predicted to increase by 2.7 and 1.4 times respectively (Fig. 12(b)), as the mass ratio of carbyne carbons to sheath carbons increases, which was higher than those of either graphene or carbon nanotubes.[94] This work also showed that LCC@SWCNT exhibit confinement-enhanced stabilities, even when they contain multiple neighboring carbyne chains, which is synthesized and observed in previous report.[95] With the development of *in-situ* TEM characterization technology, the *in-situ* research of mechanical properties of such compound system is very desirable.[96]

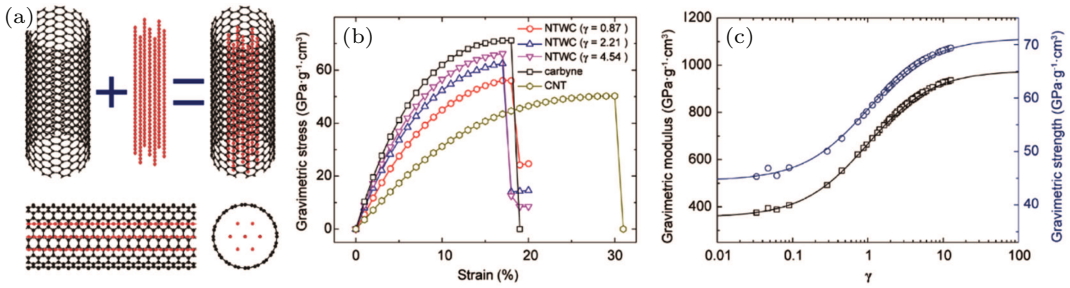

Fig. 12. (a) Illustration and longitudinal and cross-sectional views of LCCs@SWCNT. (b) Gravimetric stress–strain curves of typical LCCs@SWCNT, as compared with a carbyne chain and CNT sheath. (c) Gravimetric modulus and strength of NTWCs as a function of the mass ratio of carbyne carbons to sheath carbons, γ is linear mass densities ratio of CNT sheath and the core of carbyne chains . Reprinted with permission,[95] copyright ©2020 American Chemical Society. All rights reserved.

Except of the elastic axial tensile strain, linear response to small bending deformations and failure limits for longitudinal compression and elongation were evaluated by *ab initio* total-energy simulations, the polyynic chain is essentially as hard to compress as double-bond-based cumulene, carbyne chains turn out rigid enough that the 886-pm-long free standing polyyne can sustain a compressive strain of nearly 0.5% and 10-nN longitudinal strain before buckling.[97]

3.2. Conductance

With the significant advances in scanning tunneling microscopy (STM) and high-performance current amplifier, it is no longer an unattainable attempt for *in situ* measurement of the conductance of individual atomic chain.

Standley *et al*. observed the change of electronic transport and formation/breaking of single carbon atomic chains that bridge the junctions of two pieces of graphene.[98] After that, Wang *et al*. reported the electrical conductance of single oligoyne molecular wires using STM–molecular break junction techniques.[99] The first electrical-transport measurements of polyyne has been reported in 2013,[86] in which short chains was obtained by unraveling carbon atoms from graphene ribbons with an STM tip in a transmission electron microscopy (TEM) stage, at the same time, electrical bias was applied between the sample and the tip, and the resulting current was measured, the inherently strained polyyne exhibited a nonzero bandgap and an asymmetric shape in current–voltage curves, which is typical for rectifying behavior (Figs. 13(a)–13(c)). The relatively small value of measured conductivity is explained in terms of local strain in the chain and is also due to the contact with the graphitic electrode periphery.

After that, Torre *et al*. established electrical contacts between iron nanoparticles and short chains by similar method, the current through a carbon chain is almost a factor of 1000 lower than through the ribbon or nanotube at the same applied bias, calculated resistivity is in accordance with a previous study in the same the order of magnitude.[86] Although influenced by the low conductivity of the chain, the curve after noise fitting is almost straight, indicating the absence of a larger bandgap in this case (Figs. 13(d)–13(i)).[85]

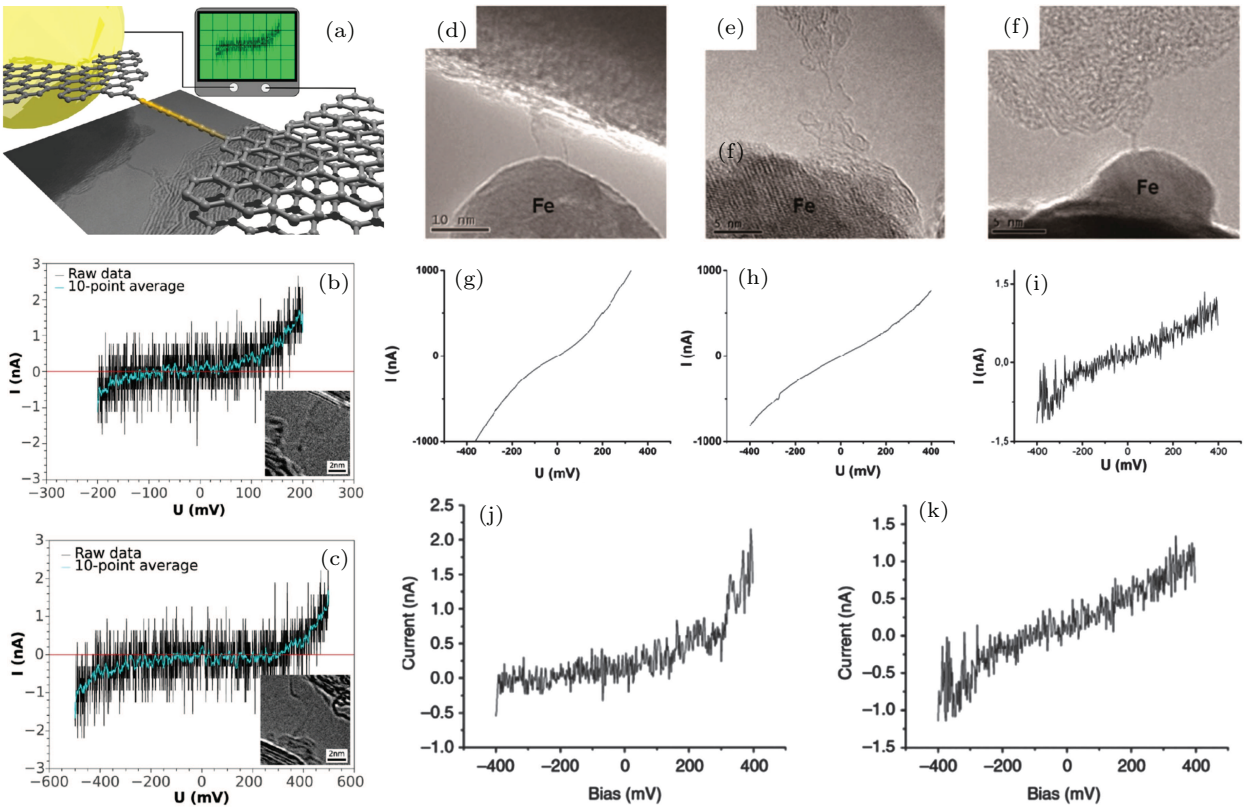

Fig. 13. (a) Illustration of *in situ* conductance measurement of monatomic carbon chain. (b)–(c) *I*–*V* measurements on two monatomic carbon chains. Images of the chains are displayed in the insets. Reprinted with permission,[86] copyright ©2013 American Chemical Society. All rights reserved. (d)–(i) TEM images and corresponding *I*–*V* curves of a graphene ribbon [(d) and (g)], an irregular nanotube-like object [(e) and (h)], and a monoatomic carbon chain [(f) and (i)]. Reprinted with permission,[85] copyright ©2014 Elsevier Ltd. All rights reserved. Panels [(j) and (k)] taken at different times during the recording of the image series show rectifying (j) *versus* Ohmic (k) behavior. This can be explained by a sudden release of strain due to a slight movement of one of the electrodes, leading to a semiconductor–metal transition in the chain. Reprinted with permission,[87] copyright ©Macmillan Publishers Limited. All rights reserved.

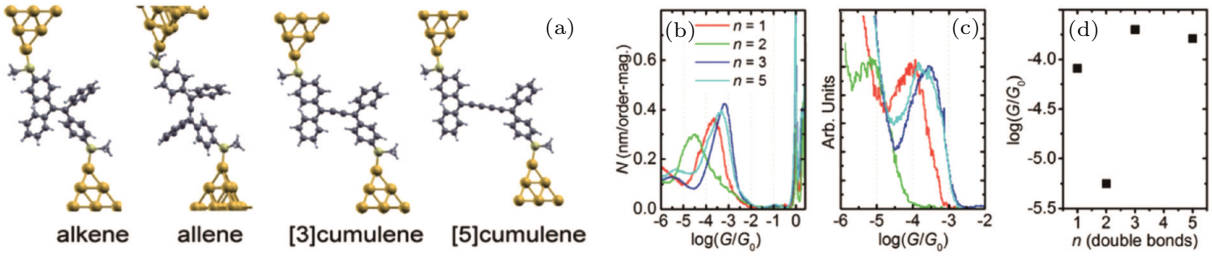

Fig. 14. (a) Calculated conformations for alkene, allene, [3]cumulene, and [5]cumulene (n = 1–5, respectively) attached to two gold leads, where the gray, white, and pale–yellow balls represent carbon, hydrogen, and sulfur, respectively. The yellow balls at both ends represent gold leads. (b) Conductance histograms using all data points. (c) The 1D conductance histogram using only points from the end of the plateau distribution. (d) Molecular conductance from Gaussian fits to the data in panel (c). Reprinted with permission,[101] copyright ©2019 Die Autoren. Verçffentlicht von Wiley-VCH Verlag GmbH & Co.KGaA, Weinheim. All rights reserved.

Inspired by the distinct phenomenon of measured conductance of carbon chains in STM, La Torre *et al*. studied the conductive behavior of short carbon chains connected with specially designed electrode, consequently, the metal–semiconductor transition in atomic carbon chains was demonstrated experimentally under strain (Figs. 13(j)–(k)),[87] and which was predicted before by Artyukhov *et al*,[100] whereas zero strain led to cumulene with ohmic behavior, the semiconducting characteristic of polyyne appeared in a strained chain.[87]

For the cumulene which was predicted to have a "metallic" electronic structure, very recently, Xu *et al*. reported the length dependence of the electrical conductivity in short cumulene with atoms chains length up to 5, and revealed that the conductance of a series of cumulenes shows remarkably little dependence on the molecular length (Fig. 14). This behavior was a consequence of the lack of strong BLA in these compounds, which would result in a steep reduction in the HOMO–LUMO band gap with increasing length.[99,101]

However, it is also worth noting that several studies have shown semiconducting character in solution-processed cumulenic thin film. Scaccabarozzi *et al*. reported the field-effect transistor (FET) fabricated employing cumulenic sp-carbon atomic wires as a semiconductor material.[102] Very recently, Pecorario *et al*. also demonstrated the solution-processed thin films and FET of tetraphenyl cumulene, the

large films providing transistors with hole mobilities in excess of 0.1 $cm^2 \cdot V^{-1} \cdot s^{-1}$, as well as promising operational stability under dark conditions.[103]

3.3. Magnetism

Conventional ferromagnetic materials always carry 3d and 4f orbital electrons. On the other hand, serval carbon allotropes only contain s and p orbital electrons also possessed weak ferromagnetic properties with the potential applications in spintronics. Magnetic ordering has been found in carbon nanofoams,[104] highly oriented pyrolytic graphite,[105] and nanocarbon films,[106] while paramagnetism is detected in amorphous carbon nanofiber,[107] nanodiamonds,[105] and graphene.[108] For those carbon allotropes consisted of the sp^2-hybridized carbon atoms, their origins of magnetism are owing to the point defects or zigzag edges of the graphene layers,[88] while nano diamonds composed of the sp^3-hybridized carbon atoms are concerned with the presence of unpaired electrons of permanent defect "color center".[105] In 2003, Chen studied electronic and transport properties of the LCC@SWCNT compound system with the tight-binding calculations, which suggested a great possibility of ferromagnetism for the combined system.[109] The spin polarized electronic transport in monatomic carbon chains covalently connected to graphene nanoribbons has also been predicted in 2010.[110] In 2013, Liu *et al*. predicted that the sp-hybridized carbon chains can be switched into a magnetic semiconductor under mechanical twisting and appropriate termination.[88] And there have been few reports about the magnetism properties of carbyne so far.

Recently, Yang *et al*. reported the paramagnetism of carbyne crystals for the first time,[111] which is synthesis by laser ablation in alcohol liquids. The collective factors containing the hydrogen atom adsorbed on the carbon chain and vacancy in crystals are suggested to be responsible for the magnetic moments.

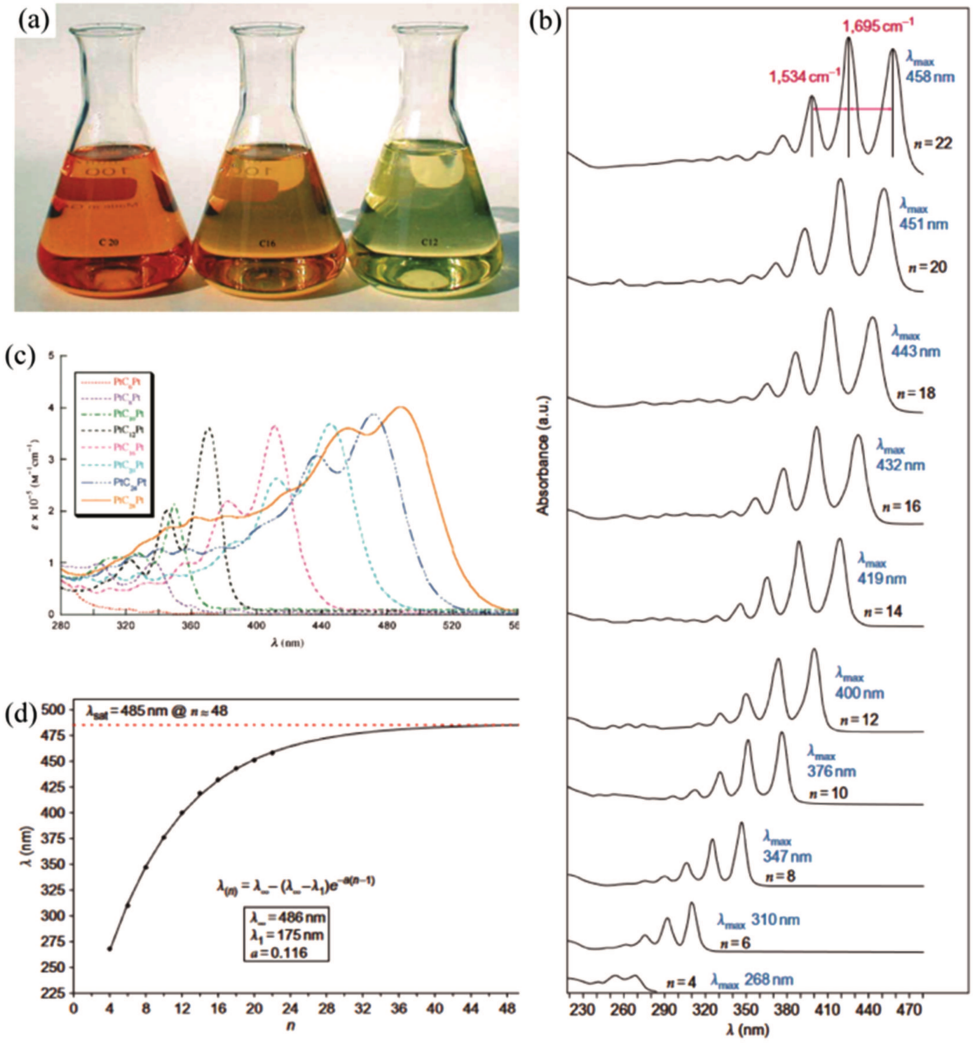

Fig. 15. (a) Solutions of compounds C_{20}, C_{16}, and C_{12} with different chain lengths in hexane/ethyl acetate 7:3. Reprinted with permission,[115] copyright ©2002 WILEY-VCH Verlag GmbH, 69451 Weinheim, Germany. All rights reserved. (b) UV-Vis spectra of polyynes with different chain lengths as measured in hexanes; wavelength of λ_{max} for each derivative is shown in blue and vibrational separations of the lowest energy absorptions are shown in magenta. (c) UV-Vis spectra of Pt end-capped polyynes with different chain lengths. Reprinted with permission,[120] copyright ©2006WILEY-VCH Verlag GmbH, 69451 Weinheim, Germany. All rights reserved. (d) Convergence of the absorption maxima λ_{max} of the series of polyynes in panel (b). [(b) and (d)] Reprinted with permission,[112] copyright ©2010 Macmillan Publishers Limited. All rights reserved.

3.4. Optical properties and spectroscopic characteristic: Light absorption, emission, and scattering

The HOMO→LUMO band gap (E_g) in polyyne depends on $\pi \rightarrow \pi^*$ transition of the C≡C bond. Thus UV-vis spectroscopy acts as a primary character in the characterization of polyyne, because these molecules typically display well resolved spectra with distinctive vibrational fine structures.[112–114] The lowest energy wavelength of significant absorption peak, λ_{max}, showed a steady red shift with increasing length, documented the lowering of the E_g (Figs. 15(a) and 15(b)).

Numerous studies used λ_{max} values for shorter polyynes with $n = 2$–16 as a predictive tool for carbyne based on the premise that the HOMO–LUMO bandgap should eventually reach an asymptotic limit with increasing length, thus the $\lambda_{max} = \lambda_{sat}$,[22,115–120] in which chain's length was marked as number of triple bonds n. At this point, λ_{sat} would also be an estimate of the HOMO–LUMO band gap.

Eisler *et al*. reported that UV-vis spectroscopy of the *i*-Pr_3Si–$[CC]_n$–Si*i*-Pr_3 polyyne with $n = 1$–7 showed a consistent lowering of E_g as a function of n, fitting a power-law relationship of $E_g \sim n^{-0.38}$,[117] and the predicted the value of $\lambda_{sat} = 570$ nm, this value matches well with the estimated $\lambda_{sat} = 569$ nm in aryl end-capped polyyne given by Gibtner *et al*,[115] as well as $\lambda_{sat} = 573$ in platinum end-capped chains reported by Zheng *et al.* (Fig. 15(c)).[120] Depending on the model used for such extrapolations, estimated values of 2.18 eV–2.56 eV have been reported for the absorption onset of carbyne.[31,112,121]

On the other hand, weak bands which observed at lower energy than the λ_{max} in UV-vis spectroscopy with various end-capped polyynes were described empirically originated from impurities[122] or orbital mixing with the terminal substituents.[115,120] Recently, Zirzlmeier *et al*. suggested that these bands can be attributed to two overlapping weakly allowed transition ($S_0 \rightarrow S_{2/3}$) to degenerate state of the trotaxane end-capped polyynes.[123] On this basis, the optical gap of polyynes was estimated to $E_g = 1.5$ eV–1.6 eV, which was 0.6 eV–0.7 eV smaller than previous estimates based on λ_{max} (Fig. 16).[123]

As the LCC@CNT, the weak absorption of LCCs is overlapped and completely covered by the strong absorption of the CNTs, thus the conurbations from LCC are hard to recognize.[124–126]

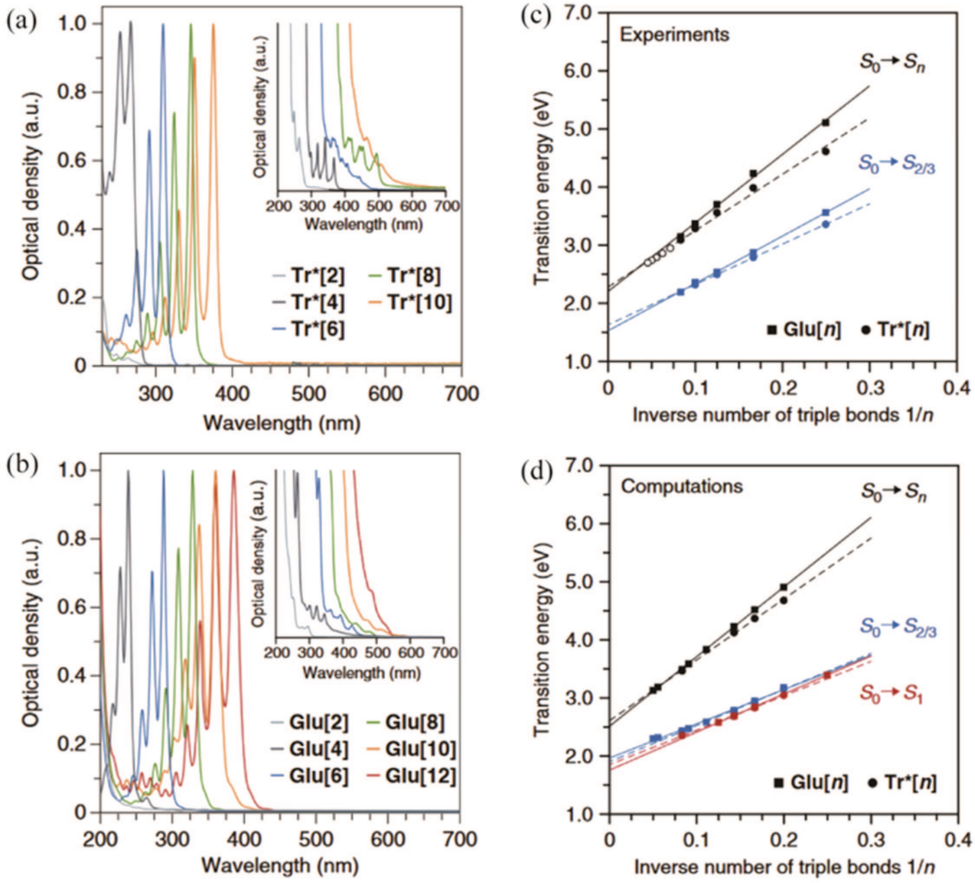

Fig. 16. (a)–(b) Absorption spectra of two homologous series of trotaxane end-capped polyynes: Tr*[n] and (b) the Glu[n]. Normalized absorption spectra of Tr*[n] (a) and the Glu[n] (b) the series recorded in hexane and acetonitrile, respectively. The insets show the additional bands with weak intensity at wavelengths higher than the absorption maximum (λ_{max}). (c)–(d) Extrapolation of experimental and computational transition energies. Plot of the energies of the experimentally determined $S_0 \rightarrow S_n$ (main) transitions and the $S_0 \rightarrow S_{2/3}$ (weakly allowed) transitions against the inverse number of carbon–carbon triple bonds $1/n$ for Glu[n] in DCM and Tr*[n] in hexane. Reprinted with permission,[123] copyright ©2020, The Author(s). All rights reserved.

Zirzlmeier *et al*. recorded fluorescence and excitation spectra of the glycosylated polyynes in hexane solutions, in which fluorescence spectra were almost mirror images of the λ_{max} bands in the absorption spectra, and the corresponding excitation spectra were exact matches of the latter (Fig. 17). By comparing absorption and emission spectra, the stokes shifts as small as 280 cm^{-1} were derived in chains with different lengths, which can be explained with the structural rigidity of oligoynes and little bond length changes upon excitation.

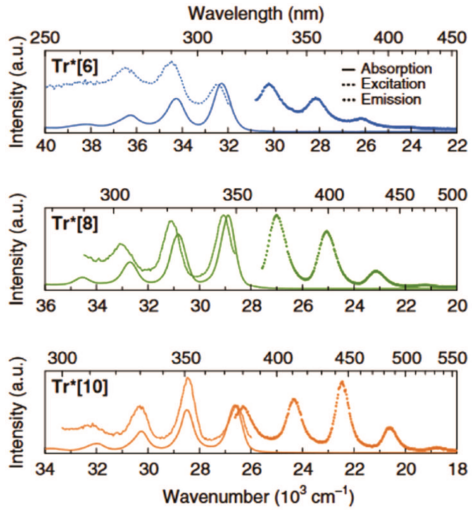

Fig. 17. Absorption (solid line), emission (dotted line), and excitation (dashed line) spectra in hexane of Tr*[6] (em. $\lambda_{exc} = 290$ nm; excitation: $\lambda = 355$ nm), Tr*[8] (emission: $\lambda_{exc} = 320$ nm; excitation: $\lambda = 400$ nm), and Tr*[10] (emission: $\lambda_{exc} = 330$ nm; excitation: $\lambda = 446$ nm). Reprinted with permission,[123] copyright ©2020, The Author(s). All rights reserved.

In the case of carbyne crystals, Pan *et al*. reported the synthesis and PL mission (Fig. 18(a)) of hexagonal crystal powder,[1] afterwards, four-color photoluminescence, and cathodoluminescence in the range from ultraviolet to near-infrared was observed,[127] as shown in Figs. 18(b) and 18(c) and the different emission center was assigned to carbyne molecules with various chain lengths.

Kutrovskaya *et al*. also observed fine structures in photoluminescence spectra of hexagonal carbyne crystals stabilized by gold nanoparticles, in which triplet peak in photoluminescence spectra was invariably composed of a sharp intense peak accompanied by two broader satellites situated 15 meV and 40 meV below the main peak (Figs. 18(d) and 18(e)), and the triplet peak repeated themselves for carbon chains of different lengths, these resonances were explained as the emission of edge-state neutral, positively and negatively charged excitons, respectively (Figs. 18(f)–18(j)).[128] Very recently, Kutrovskaya *et al*. found that the excitonic fine structure was governed by the interplay between the hopping energy in a Van der Waals quasicrystal, neutral-charged exciton splitting, and positive–negative exciton splitting (Fig. 18(k)).[129]

Raman spectroscopy has been used in many studies to confirm the presence of confined LCC in CNTs, with the fingerprint Raman peak "C-mode" was found to appear in the range between 1790 cm^{-1} and 1860 cm^{-1}.[13,67,130–132] Shi *et al*. have confirmed that the C-mode frequency and length of short chains are linearly related, but for the long linear chains beyond $\sim$ 100 atoms confined in CNT, as shown with black dashed line in Fig. 19(a), the C-mode frequency do not exhibit any length-dependence, indicating that the chains more than 100 atoms can be considered as a finite realization of carbyne.[133] Immediately, Shi *et al*. recorded such Raman resonance profiles of six C-mode frequency bands in the range between 1793 cm^{-1} and 1856 cm^{-1} from LCC@DWCNTs and have shown that each Raman peak can be associated with a different bandgap (Figs. 19(b)–19(e)).[134] The relationship between Raman frequency, band gap, and chain length have been established. This means that researchers can estimate the length and band gap of the chain from the C-mode frequency, which greatly facilitating the study under various conditions.[135]

For the short colloidal polyynic chains, similar linear relationship between the chain length and C-mode frequency was confirmed by both experimental and theoretical,[119,136,137] Compared with the endcapped polyynic chains, the frequency of C-mode band in LCC@CNT was shifted by 120 cm^{-1}–290 cm^{-1} under strong effect of Van der Waals interaction of CNT.[133] Otherwise, for the short sp-hybridized carbon chains with a few carbon atoms, the resonant wavelength of energy gap located at UV range,[138] which is far away from the common excited laser source used in Raman spectrometer. And the concentration of Polyynes in organic solvent is usually very low aimed for stable preservation, it is difficult to obtain a good signal-to-noise ratio Raman signal by using the commonly used Raman. In order to obtain polyyne Raman spectra using Ar^+ laser (wavelength 514 nm), Tabata *et al*. increased the laser power to 600 mW and removed the n-hexane background signal to obtain a good signal-to-noise ratio.[119]

For the another hexagonal carbyne crystals, the polycrystalline powder named "white carbon" shows different Raman characters, which manifest as two prominent Raman band localized at 1060 cm^{-1} and 2100 cm^{-1}, Pan and coworkers suggested these peak was generated from the in panel stretching vibration mode of single and triple bonds by carbon–carbon triple bonds, respectively.[1,127] It is still a question worthy for exploring whether the reason for the significant difference is caused by the chains in different atomic environments.

The information accessible by Raman spectroscopy is not limited to vibrational properties. For instance, resonant enhancement of Raman scattering occurs for excitation energies close to or coinciding with an optical transition. Therefore, by recording the Raman signal as a function of excitation energy, information about the electronic structure can be obtained as precise as the range of 20 meV. This allows not only the measurement of band gaps,[134] but also further analyses of the

fine structure of the electronic transitions and vibronic series of optically allowed transitions. Very recently, Martinati *et al*. investigated the excited states of the LCC@DWCNTs with resonant Raman spectroscopy, in addition to the optical band gap, the Raman resonance profile shows three additional resonances, which was assigned to a vibronic series of a different electronic states separated by an energy range of 0.14 eV–0.22 eV.[139]

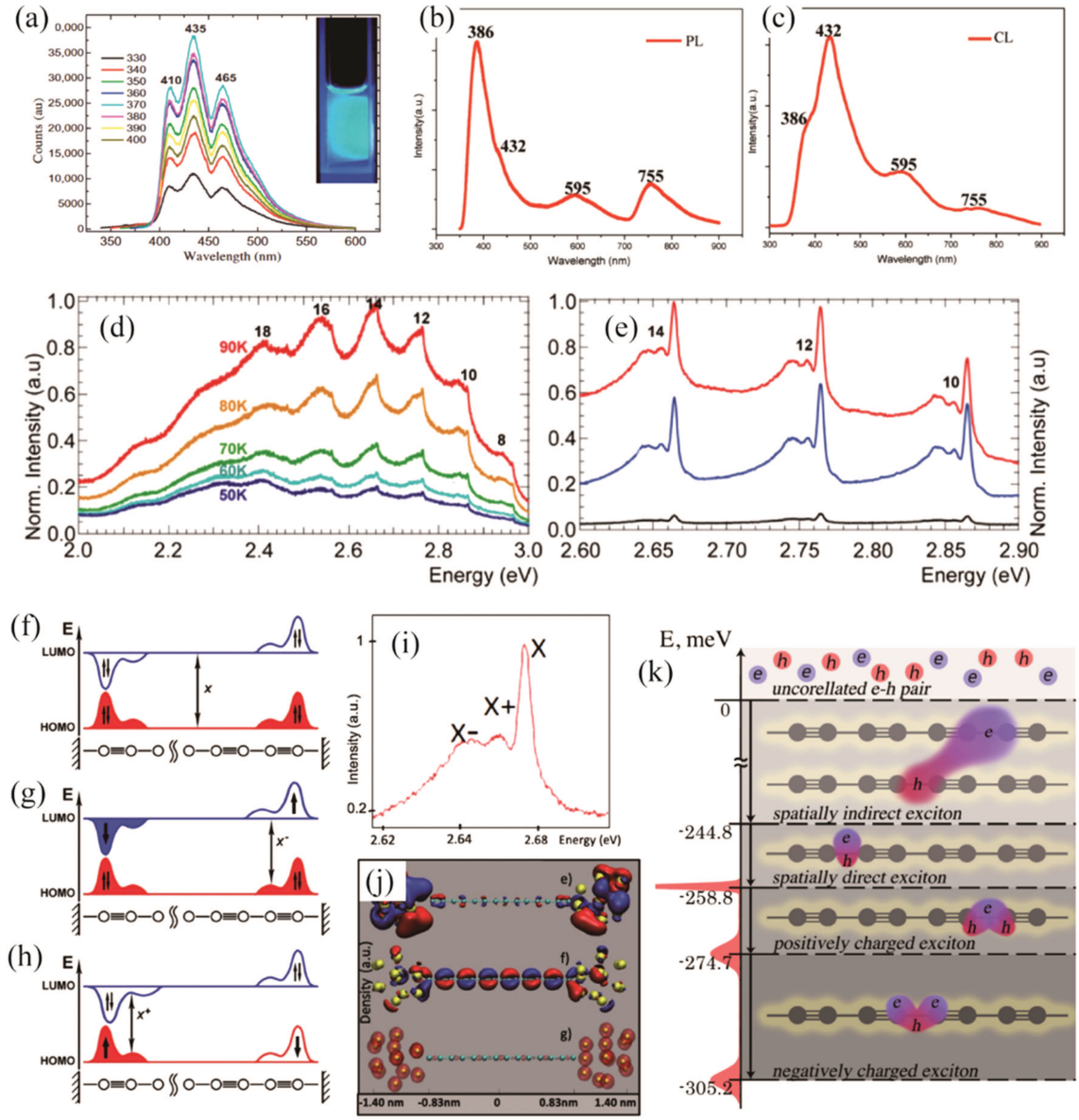

Fig. 18. Emission from carbyne crystals. (a) Three fluorescence peaks (at 410 nm, 435 nm, and 465 nm) remain the same as excitation wavelength varies. Inset: The purple–blue fluorescence graph excited with a 370-nm light. Reprinted with permission,[1] copyright ©2015 American Association for the Advancement of Science. All rights reserved. (b)–(c) PL (excited at 325 nm) and CL characterizations of the synthesized carbyne crystals, note that these four peaks are identical to the PL spectrum. (d)–(e) PL spectra of the deposited carbyne crystals of different lengths (the number of atoms in the chain is indicated on the top of the corresponding spectral resonance). Reprinted with permission,[127] copyright ©2017 Wiley-VCH Verlag GmbH & Co. KGaA, Weinheim All rights reserved. (d) Spectra taken at temperatures from 90 K to 50 K (red 90 K, yellow 80 K, green 70 K, teal 60 K, and blue 50 K). The laser excitation wavelength is 390 nm with the intensity of 5 mW and the acquisition time of 10 s. (e) PL spectra taken at 4 K. Red, blue, and black curves correspond to the excitation wavelengths of 390 nm, 380 nm, and 370 nm, respectively. The acquisition time is 40 s. (f)–(k) Scheme of excitonic transitions in carbyne crystals. (f) The neutral exciton (X) is formed by even and odd edge states that originate from the HOMO–LUMO pair. (g)–(h) Trion transitions in charged chains, where the left–right symmetry is broken so that the optical transition occurs either between the original HOMO state and the spin-polarized electron state localized at one of the edges (X−) or between the hole state localized at one of the edges and the original LUMO state (X+). (i) Enlarged PL spectrum of a characteristic triplet corresponding to the 14-atom chain that shows the relative strengths of exciton and trion transitions. Molecular orbitals and total electron density plots for a model system containing a polyyne chain composed of 14 carbon atoms capped with two gold NPs for HOMO (e) and LUMO (f). (g) Total calculated electron density. Red and blue lobes correspond to positive and negative values, respectively. Reprinted with permission,[128] copyright ©2020 American Chemical Society. All rights reserved. (k) The schematic energy diagram explaining the triple PL structure. Photoexcited electrons and holes may form spatially indirect excitons that do not emit light, as well as charged and neutral spatially direct excitons. The calculated transition energies of direct and indirect excitons as well as X^+ and X^- trions are indicated with respect to the transition energy between uncorrelated electron and hole states. Reprinted with permission,[129] copyright ©2021 American Physical Society. All rights reserved.

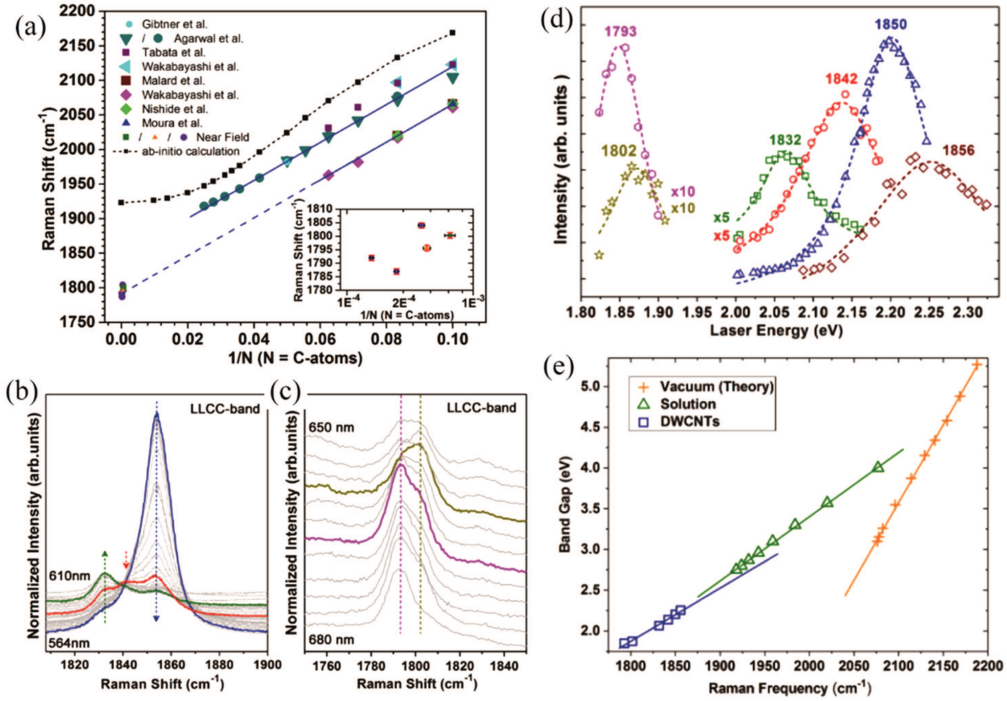

Fig. 19. (a) Raman response of polyynes and LCC@CNTs as a function of inverse length, given by the number N of carbon atoms. The solid lines are linear fits to the available data on chains with assigned lengths (upper solid line: colloidal chains, lower solid line: LCC@CNTs, dashed blue line: extrapolation to infinite chains). The inset shows data derived from near-field Raman microscopy images. Reprinted with permission,[133] copyright ©2016 American Physical Society. All rights reserved. (b)–(c) The evolution of the Raman spectra of LCC@DWCNTs excited by lasers with a wavelength 564 nm–610 nm (b) and 650 nm–680 nm (c). The resonance Raman spectra for the LCC peaks at 1793, 1802, 1832, 1842, as well as the sum of 1850 cm^{-1} and 1856 cm^{-1} were highlighted by magenta, dark yellow, olive, red, and blue lines, respectively. (d)–(e) Resonance Raman excitation profiles for six LCC band peaks. The dashed lines are a fit to the experimental data. (b) Band gap of the LCCs as a function of Raman frequency of the LCCs. The orange crosses are theoretical prediction by *ab initio* calculations on the free chains in vacuum, the olive triangles represent LCCs terminated by bulky end groups in toluene (Raman frequencies) or hexane (band gap), and the blue squares are our work on LCCs inside DWCNTs. The linear lines are the fittings of the data points. Reprinted with permission,[134] copyright ©2017 American Physical Society. All rights reserved.

However, as in any conventional optical microscopy technique, the spatial resolution of Raman spectroscopy is fundamentally limited by diffraction, which is insufficient for resolving and characterizing the morphology of carbyne.[140,141] TERS spectrometer equips with an optical nanoantenna havs enabled Raman spectroscopy to be performed with spatial resolution down to 10 nm, and weak signal intensity of monodisperse sample with conventional far-field measurements technology have been overcome trough this technique. *In situ* Raman-AFM mapping of the longest LCC correlated to length of more than 6000 carbon atoms was observed using TERS.[14] More than that, Tschannen *et al*. investigated the anti-Stokes Raman mode in LCC@CNTs and the temperature dependence of the and anti-Stokes/Stokes ratio, provides a means for all optical probing temperature sensing on the nanoscale.[142]

4. The modifications under different external conditions

Fundamentally, the electronic structure of carbon chain is determined by its BLA value. Many factors can affect the BLA, for example, the length of the chain, temperature, pressure, mechanical deformation: bending, axial stress and compress, the effects of end-group and encapsulation by CNTs also needs to be considered. Therefore, many previously theoretical studies concentrated on investigating the end-group effect, bending effect, and charge transfer with substrate, *etc*.[88,143–147] Servals changes of physical quantities have also been observed experimentally. In the following, those factors will be discussed in detail.

4.1. Temperature

As well known, materials always undergo phase transitions with the verified temperature and pressure. But for the truly one dimensional carbyne, the structural evolution was driven by the the strength of bond and BLA value caused by the Peierls distortion.[2]

Wong *et al*. developed a Monte Carlo algorithm of the carbon chains from 1 K to 1300 K, observed the bond softening at 500 K and the bond soften behavior does not change with the length of nanowire.[148] Yang *et al*. found the ultimate strength, Young's modulus and maximum strain of carbyne are rather sensitive to the temperature and all decrease with the temperature.[149]

Lin *et al*. reported the Peierls distortion in carbyne was strongly related to temperature, a surprisingly huge distortion was found in the carbon atomic chains created in TEM at 773 K (Figs. 20(a)–20(d)), and the abnormally distorted phase only dominates at the elevated temperatures, while the distorted and undistorted phase coexisted at ambient temperature (Figs. 20(e)–20(j)).[150]

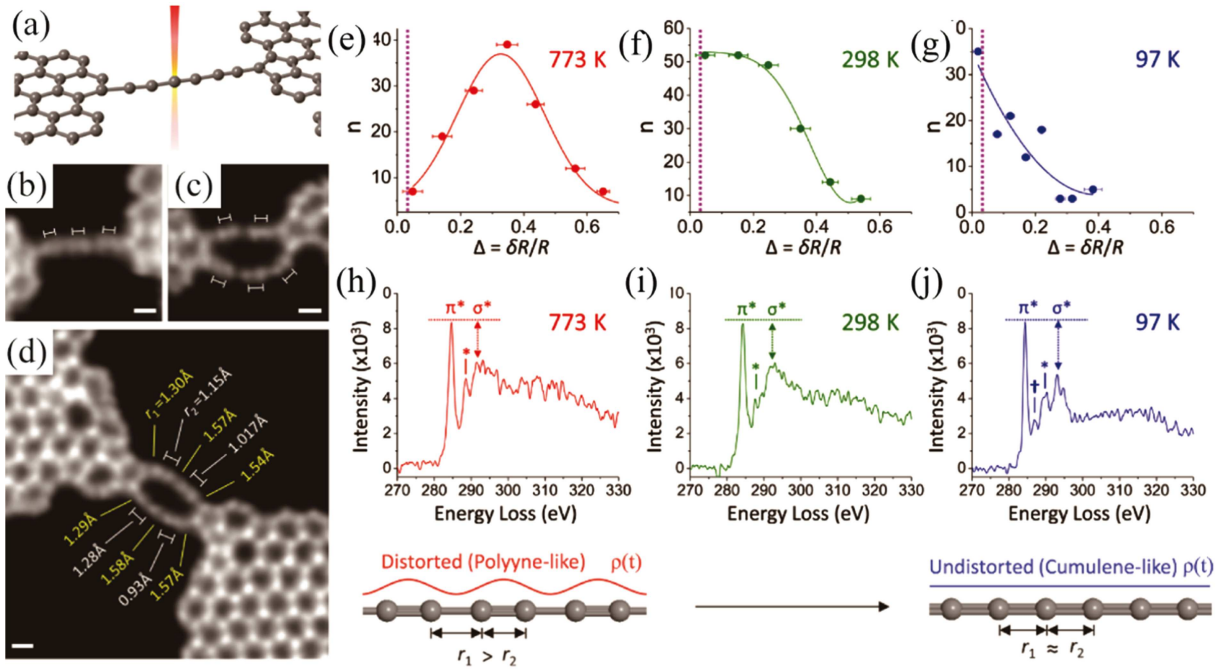

Fig. 20. (a) Schematic diagram of a suspended carbon chain created and studied by electron beam. (b)–(d) Experimental evidence of largely dimerized carbon chains at 773 K by atomic resolution annular dark field imaging, scale bars are 2 Å. (e)–(g) Statistical dimerization ratio of carbon chain at 773 K, 298 K, and 97 K. Purple vertical dotted line indicates the theoretical value of an ideal infinite polyyne (BLA=0.03). (h)–(j) The electron energy-loss spectra (EELS) of carbon chain at 773 K (red curve), 298 K (green curve), and 97 K (blue curve). Each spectrum was averaged by five EELS line scans across the middle of carbon chains. Reprinted with permission,[150] copyright ©2016 American Chemical Society. All rights reserved.

4.2. Pressure

Hydrostatic pressure, as an important and clean external stimulus, can modify the electronic and structural properties of materials without introducing any impurity or additional groups. Note that Liu's group is one of the five research groups internationally to break the limit of commercial large-volume press and achieve 30 GPa at high temperature with the WC anvil so far.[151] This makes China become the third country in the word to hold such key technology, after Japan and Germany. High-pressure technique has been introduced to focus on the mechanical, electronic, and vibrational properties of carbon materials, as well as their interactions between graphene sheets, concentric tubes in MWCNTs and/or bundled CNTs.[152–157]

For the most of the carbon chains that exist stably in solid form are packaged in CNT, and to prevent the end groups from participating in the reaction with carbon chains under high pressure, the high-pressure of carbon chains studies are mainly concentrated in the system of LCC@CNTs.

Andrade first reported a pressure-induced coalescence of adjacent chains encapsulated in multi-walled carbon nanotubes, increasing the carbon chain length from 9 to 40 atoms.[158] Neves *et al*. show that the short carbon chains with around 36 carbon atoms inside DWCNTs exhibit an irreversible cross-linking between inner tubes and chains under high pressure, in which the pressure range is probed between 19.2 GPa and 39.2 GPa when chain-inner tube cross-linking occurs (Figs. 21(a) and 21(b)).[159]

After the successfully synthesized of the ultralong LCCs with more than 6000 atoms, which offers a perfect candidate to study the band gap evolution of carbyne under high pressure, Yang *et al*. showed that the vibrational modes and band gaps of LCC@CNTs reduce with the increased pressure (Figs. 21(c) and 21(d)), theoretical simulations confirmed that the reduction of BLA with increasing pressure is responsible for the pressure-induced bandgap decrease (Fig. 21(e)). And cross-linking reaction between the inner tube and the chain occurred at around 53 GPa (Fig. 21(f)),[135] which is higher than the pressure value than short chains in Andrade's report, implied that the long LLC@CNTs with long chains possess a greater pressure stability than the short chains.[158] Very recently, Neves *et al*. compared the pressure-induced structural transformations on chains of different length inside DWCNTs, which shows that coalescence between the shorter chains occurs in a region of lower pressure than that of the longer chains.[160]

In addition, through systematic analyzing of the softens behavior of LCCs' spectroscopic signature Raman band with increasing pressure. Sharma *et al*. proposed an anharmonic force-constant model based on the anharmonic nature of carbon–carbon (C–C) single bonds to describe the change of mechanical properties from the soften behavior of Raman mode under pressure, which showed that the LCCs' Young's modulus (E), Grüneisen parameter (γ), and strain (ε) follow universal P^{-1} and P^2 laws, respectively (Fig. 22).[161]

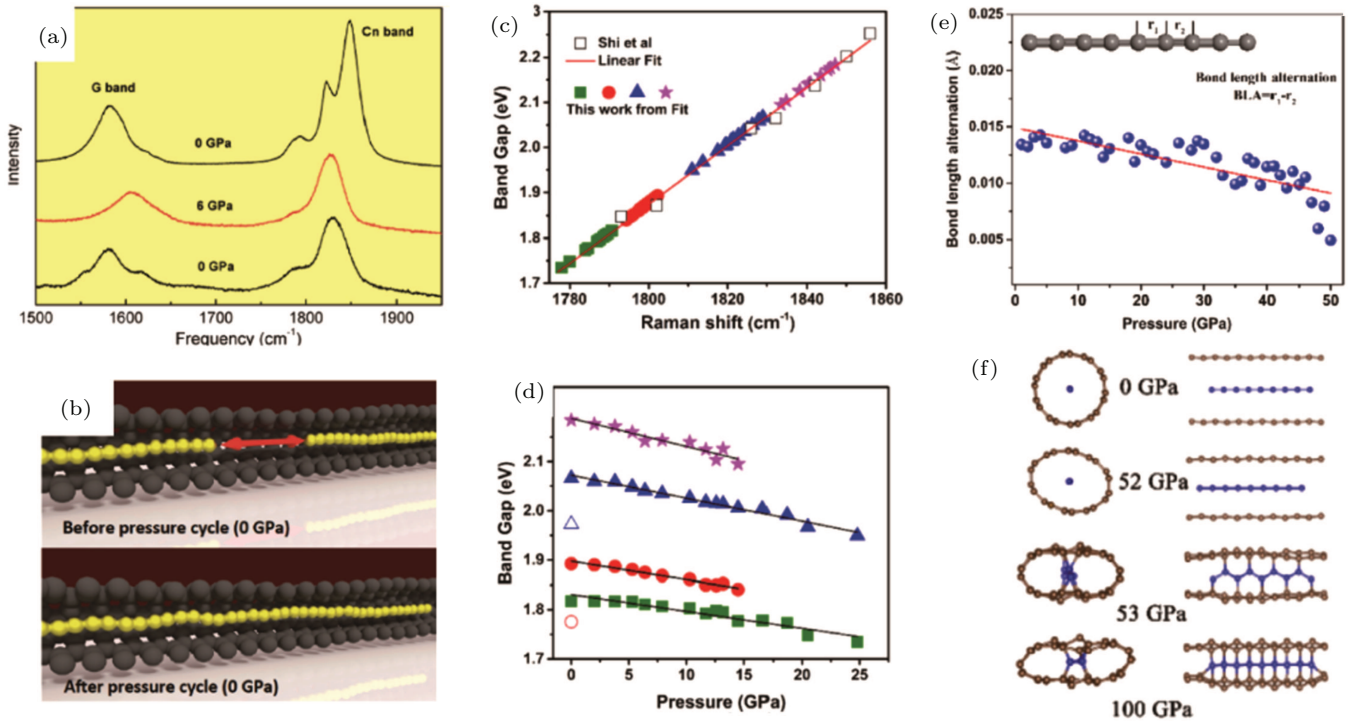

Fig. 21. (a) Raman spectra recorded at 9 GPa, 6 GPa, 3 GPa, and 0 GPa and outside the cell before compression. (b) Representation of the linear carbon chain (in yellow) confined inside the carbon nanotubes, the red double arrow indicates the chain separation before the increase of the external pressure value, pressure induces the coalescence of the two chains. [(c) and (d)] Band gap evolution of LCC under pressure. Reprinted with permission,[158] copyright ©2015 Elsevier Ltd. All rights reserved. (c) A linear fited data of band gaps of LCCs as a function of Raman frequency was used to calculate the band gaps of the LCCs under different pressure. (d) The predicted band gaps of the LCCs (shown in different shapes) as a function of pressure during compression (solid symbols) and decompression (empty symbols). (e) The BLA as a function of pressure. Inset shows the molecular structure of carbon chain. (b) Simulations for the deformation of LCCs@DWCNTs at selected pressures. Reprinted with permission,[135] copyright ©2020 Elsevier Ltd. All rights reserved.

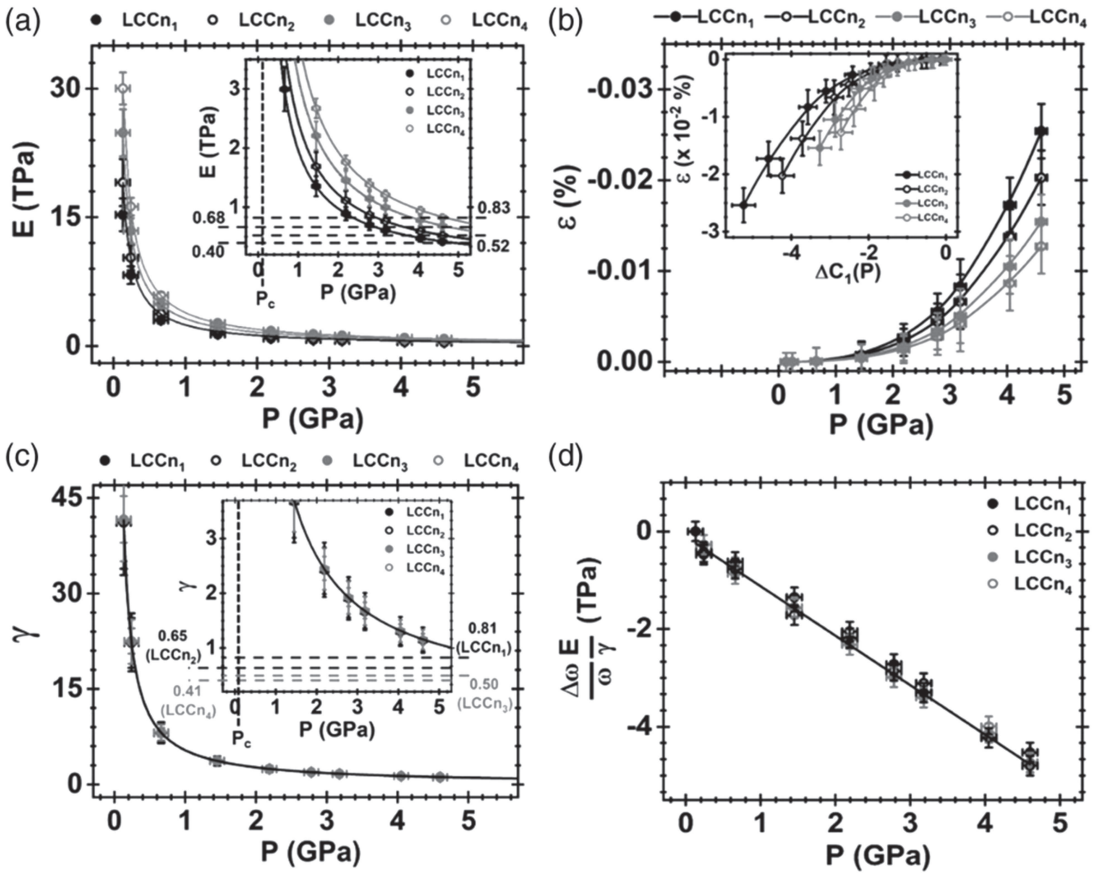

Fig. 22. Experimental data fittings under pressure. (a) Young's modulus E, (b) strain ε, and (c) Grüneisen parameter γ as a function of P for each LCC. Both E and γ follow a P^{-1} universal law, while ε follows a P^2 universal law. (d) $(\Delta\omega/\omega)$ $(E/\gamma) = -P$, an important parameter for nanometrology, is universal and unified. Reprinted with permission,[161] copyright ©2020 American Physical Society. All rights reserved.

4.3. Mechanical deformation: Axial stretching and compression, bending and twisting

Under tension force along axis direction, carbyne was predicted to be as stiff as the strongest one-dimensional materials.[88] Hu *et al*. also investigated the bending effect of polyynic chains with DFT calculations (Fig. 23(a)), it was found that the HOMO–LUMO energy gap of the polyynic chain was decreased, whereas the gap of the cumulenic chain remained almost unchanged with increasing the bending (Fig. 23(b)). Furthermore, the chains can be easily bent with a small arc-chord ratio, strain energy even due to a large bending was still much smaller than the energy required for breaking bonds in a chain, in other words, the chain presented like nano-rope was relatively easy to bend but hard to break.[144]

With excellent strength under tensile loading, the carbon chain readily buckles under compressive loading. It was found that under the bracing effect of confinement in CNTs with chirality of (6,6), (7,7), and (8,8), LCC can buckle into a coiled helix-shaped nano-spring (Fig. 24) and followed Hooke's law under axial compression.[162]

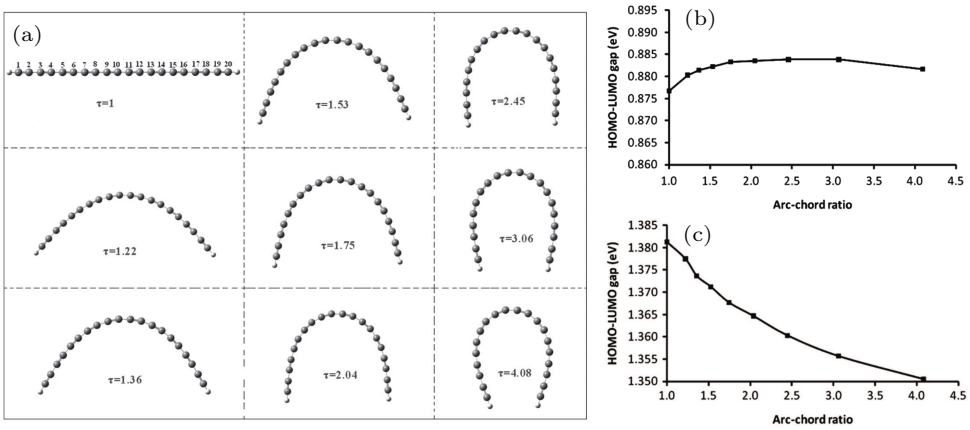

Fig. 23. (a) Straight and bent polyynic ($C_{20}H_2$) chains with various arc-chord ratios (τ). (b) and (c) Band gap of bent polyynic (b) and cumulenic (c) chains *versus* arc-chord ratios. Reprinted with permission,[144] copyright ©2011 American Chemical Society. All rights reserved.

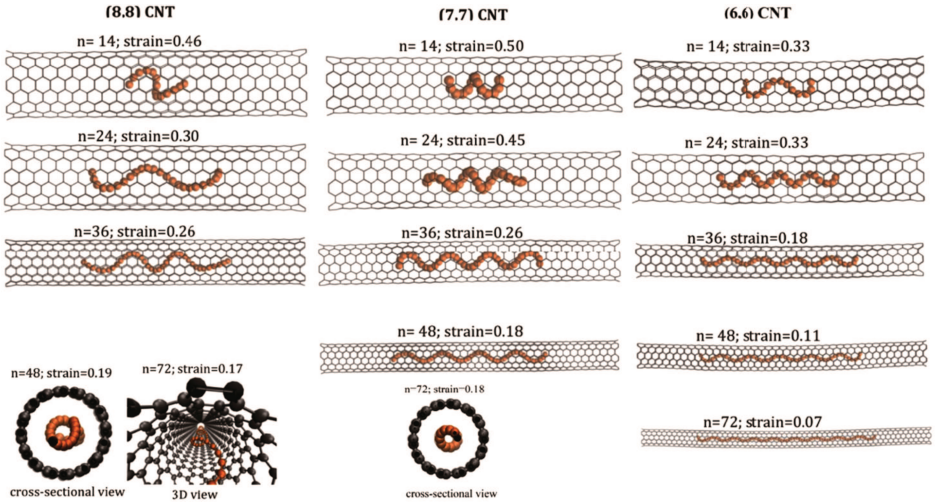

Fig. 24. Forming of helix-type springs of carbyne chains inside (6,6), (7,7), and (8,8) CNTs. Reprinted with permission,[162] copyright ©2019 Elsevier B.V. All rights reserved.

Interestingly, it was predicted that a metal–semiconductor transition would occurs at about 3% tensile strain, and has been confirmed experimentally.[87,88] The effect on electronic properties is more pronounced when twisting is imposed on the end groups compared with the chain's skeleton. Liu *et al*. compared different functional groups, including methyl (CH_3), phenyl (C_6H_5), and hydroxyl (OH) as sp^3 radicals and amine (NH_2, planar) and methylene (CH_2) groups from the sp^2 family. With methyl and hydroxyl, the single C–C bond at the end interfaces result in a completely free unhindered rotation. Only the polyynic chains with sp^2 terminations like CH_2 and NH_2 acted as the "handles" showed a detectable torsional stiffness. As shown in Fig. 25(d), with increasing torsional angle, the band gap of methylene end-capped polyynic chain shrank and completely closed at 90°.[88] Ravagnan *et al*. performed ab initio total-energy and phonon calculations on polyynic chains with sp^2 graphite terminations, suggested twisting would modify the electronic states near the Fermi level, and predicated the possibility to control the nanowire conductance with micromachined torsional actuators.[163] In addition, the mechanical

twisting induced negative differential resistance, spin polarization and magnetic semiconductor state switching have also been predicated.[88,164]

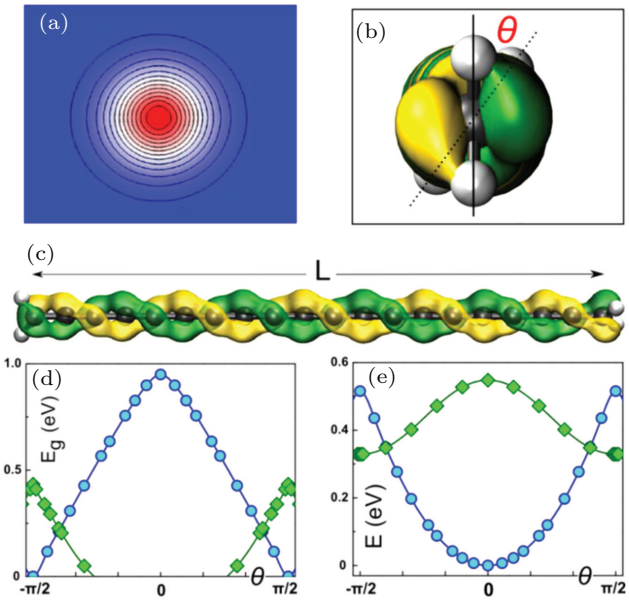

Fig. 25. End-group-induced torsional stiffness of carbyne. (a) Cross section of the electronic density of carbyne. (b) Front and (c) side views of a carbyne chain with attached CH_2 handles, showing the helical HOMO isosurface. (d) Band gap and (e) energy as a function of the torsional angle: blue, singlet state; green, triplet. Reprinted with permission,[88] copyright ©2013 American Chemical Society. All rights reserved.

4.4. Terminal end groups

Basically, introducing bulky end-groups can provide steric hindrance to prevent the cross-linking reactions among the polyynic chains. Experimental synthetic efforts were already paid on preparing various of heteroatom end-capped polyynes, such as hydrogen, alkyl, aryl, trialkylsilyl, and metal.[24,26–29,31,33,35,165] Hydrogen or methyl caps are the simplest ones for short polyynes, however, not good enough for stabilizing long polyynes. Organic groups with larger molecular weights are more effective in this case, using trismethyl as the end group, the longest polyynic chains up to 48 atoms has been synthesized, in which the end groups can be used both to stabilize the wire and for selecting polyyne-like vs cumulene-like structures.[9,112]

It was also believed that the modulation of the structural, electronic, and vibrational properties of the sp-carbon chain requires a suitable chemical design of the end group. Substituting the end-capping groups with electron-donating/accepting properties would tune the vibrational frequency of the polyynic chains by influencing π-electron delocalization. Hu *et al*. engineered a novel class of polyynes with 20 distinct Raman frequencies through end-capping substitution, rational engineering, and isotope doping. Based on this method, optical multiplexing imaging with 10-color organelle imaging in single living cell with high specificity, sensitivity, and photo-stability has been demonstrated.[165]

Interestingly, unsymmetric end capping groups would induce the chain polarization effects in polyynes and affect vibrational properties significantly. Agarwal *et al*. investigated the vibrational properties (FTIR and Raman) of a series of symmetrical and unsymmetrical endcapped polyynes of different chain lengths in the range of 8–40 atoms.[30] The violation of the mutual exclusion principle between infrared (IR) and Raman spectroscopy was observed, which is strictly valid only for a perfectly linear centrosymmetric chain.

4.5. Cladding CNTs for LCC@CNTs

The vibronic and electronic properties of the LCC were found to be influenced by its nanotube host significantly. Rusznyák *et al*. performed first principles calculations on an infinite LCC encapsulated inside SWCNTs along with an isolated carbon chain as reference. It was shown that a combined effect of hybridization and charge transfer leads to a partial suppression of the BLA when the chain is inside a tube, and that the combined systems are metallic with a high density of states at the Fermi level.[166] Tapia *et al*. also confirmed the metallic behavior by DFT study on LCC@SWCNT hybridized system, it was shown metallic conductance came from charge transfer from carbon nanotube to the LCC,[167] such electronic transfers process occurring from the nanotubes to the polyynic molecules was observed experimentally in resonance Raman spectra by Moura *et al.* (Fig. 26(a)).[168]

For the influence of cladding CNTs on mechanical properties, molecular dynamics simulation and elastic string–elastic shell model is adopted to study radial pressure-induced buckling of LCC@SWCNTs, Hu *et al*. predicated the critical buckling pressure have increases considerably with 160% maximum compared with SWCNT.[169] In return, the mechanically soften LCC under bending is indeed protected by the CNT shell upon the encapsulation. It was also found that the interaction between CNT and LCC becomes more obvious when the CNT diameter decreases.[170]

Wanko *et al*. found that the Van der Waals interaction between LCC and CNT possess strong effects on vibration properties of LCC, referenced by the intrinsic Raman frequency of polyyne in vacuum, an explicit describe of the interactions between LCC and CNT has shown a shifted the chain's Raman band by 118 cm^{-1}–290 cm^{-1}.[133] Heeg *et al*. revealed that CNT of different chirality determines the vibronic and electronic properties of the encapsulated LCC, as shown in Fig. 27, by choice of chirality, the fundamental Raman mode (C-mode) of the chain was tunable by $\sim$ 95 cm^{-1} and its band gap by $\sim$ 0.6 eV.[171]

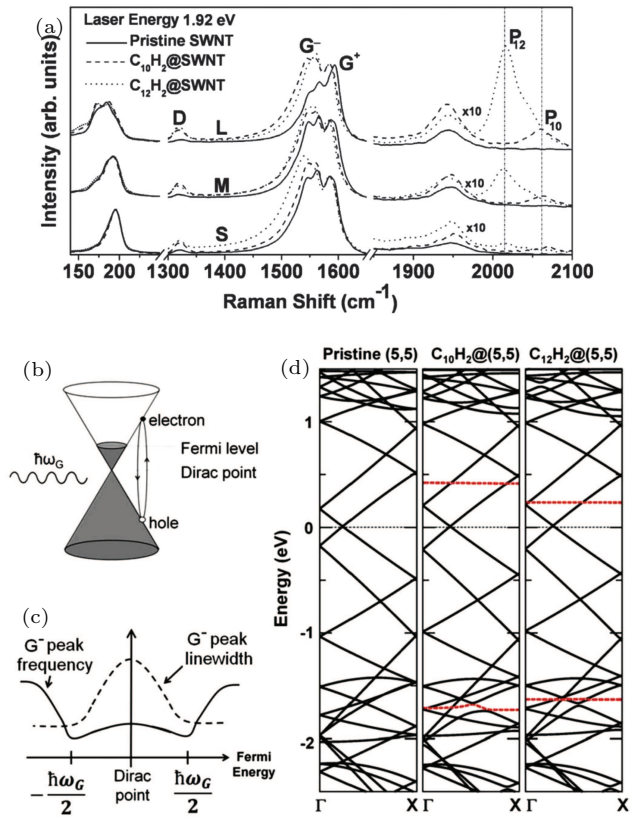

Fig. 26. (a) Raman spectra for pristine SWNTs (solid curves), $C_{10}H_2$ @ SWNT (dashed curves), and $C_{12}H_2$ @ SWNT (dotted curves) showing the RBM modes, the G band between 1500 cm^{-1} and 1600 cm^{-1} and the polyynes bands indexed by P_{12} and P_{10} between 2000 cm^{-1} and 2100 cm^{-1}. The labels L, M, and S denote SWNTs with large, medium, and small diameters, respectively. (b) Phonon assisted creation and annihilation of an electron-hole pair. (c) Frequency (full line) and the linewidth (dashed line) of the G^- peak of metallic nanotubes as a function of the Fermi-level position. (d) Electronic band structure for the pristine (5,5) SWNT, $C_{10}H_2$ @ (5,5), and $C_{12}H_{25}$. The HOMO and LUMO bands of the polyyne molecules are shown in dashed red lines. The dotted line is the Fermi level for undoped samples. Reprinted with permission,[168] copyright ©2009, The American Physical Society. All rights reserved.

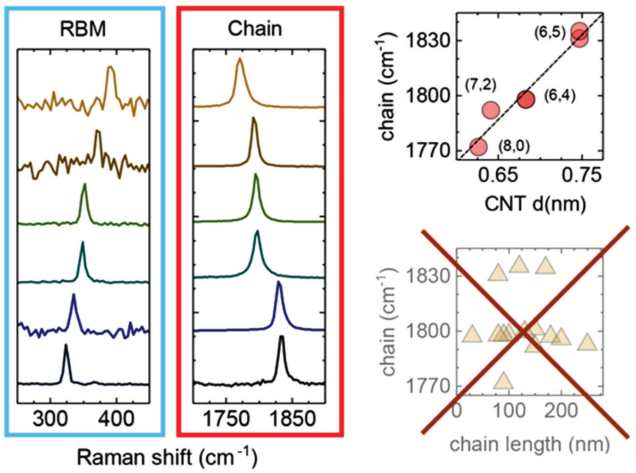

Fig. 27. Simple schematic diagram of LCC Raman frequency influenced by the CNT clarity. Reprinted with permission,[171] copyright ©2018 American Chemical Society. All rights reserved.

5. Conclusion and perspectives

In this review, we briefly introduced the different forms of carbyne synthesized in laboratory, from synthesis methods to the modifications of physical properties. Both the important discoveries of milestone and recent interesting progresses are included. The high instability of sp-hybridized bond and cross-linking effect between chains make the availability of this material in bulk quantities under ambient conditions very unlikely. So far, the stable forms of experimental samples mainly include the end-capped chains, LCC@CNTs and Van der Waals crystal of carbyne. On one hand, the poor stability of sp-carbon is still the major problem limiting its exploitation in practical applications. Thus, the experimental efforts to synthesize longer free-standing chains, and the influence of end/side contacts on the stability, must be undertaken. On the other hand, various characteristic methods have been introduced for investigating vibratory properties, the mechanical strength and conductance, but the experimental data that dovetail well with theoretical calculations was still missing. The *in-situ* synthesis and analytical method, as well as the modification of physical properties for sp-carbon are still expected.

Acknowledgements

Project supported by the National Natural Science Foundation of China (Grant Nos. 12174348 and 62027816), the China Postdoctoral Science Foundation (Grant Nos. 2018M630830 and 2019T120631), the Natural Science Foundation of Henan Province, China (Grant No. 212300410410), and the Fund from the Henan Center for Outstanding Overseas Scientists (Grant No. GZS201903).

References

[1] Pan B T, Xiao J, Li J L, Liu P, Wang C X and Yang G W 2015 *Sci. Adv.* **1** e1500857
[2] Kertesz M, Koller J and A zman 1978 *J. Chem. Phys.* **68** 2779
[3] Whittaker A G 1978 *Nature* **276** 695
[4] Casari C S, Tommasini M, Tykwinski R R and Milani A 2016 *Nanoscale* **8** 4414
[5] Casari C S and Milani A 2018 *MRS Commun.* **8** 207
[6] Karpfen A 1980 *J. Phys. C: Solid State Phys.* **13** 5673
[7] Milani A, Tommasini M, Fazzi D, Castiglioni C, Zoppo M D and Zerbi G 2008 *J. Raman Spectrosc.* **39** 164
[8] Franz M, Januszewski J A, Wendinger D, Neiss C, Movsisyan L D, Hampel F, Anderson H L, Görling A and Tykwinski R R 2015 *Angew. Chem., Int. Ed.* **54** 6645
[9] Gao Y Z, Hou Y X, Gordillo Gámez F, Ferguson M J, Casado J and Tykwinski R R 2020 *Nat. Chem.* **12** 1143
[10] Wendinger D, Januszewski J A, Hampel F and Tykwinski R R 2015 *Chem. Commun.* **51** 14877
[11] Wendinger D and Tykwinski R R 2017 *Acc. Chem. Res.* **50** 14
[12] Zhang K, Zhang Y F and Shi L 2020 *Chin. Chem. Lett.* **31** 1746
[13] Zhao X L, Ando Y, Liu Y, Jinno M and Suzuki T 2003 *Phys. Rev. Lett.* **90** 187401
[14] Shi L, Rohringer P, Suenaga K, Niimi Y, Kotakoski J, Meyer J C, Peterlik H, Wanko M, Cahangirov S, Rubio A, Lapin Z J, Novotny L, Ayala P and Pichler T 2016 *Nat. Mater.* **15** 634
[15] Jin C H, Lan H P, Peng L M, Suenaga K and Iijima S 2009 *Phys. Rev. Lett.* **102** 205501
[16] Tarakeshwar P, Buseck P R and Kroto H W 2016 *J. Phys. Chem. Lett.* **7** 1675

[17] Heimann R B, EvsyuHeimann R B, Evsyukov S E and Kavan L 1999 *Carbyne and Carbynoid Structures* (Springer Science & Business Media) p. 35

[18] Kavan L 1997 *Chem. Rev.* **97** 3061

[19] Lagow R J, Kampa J J, Wei H C, Battle S L, Genge J W, Laude D A, Harper C J, Bau R, Stevens R C, Haw J F and Munson E 1995 *Science* **267** 362

[20] McCarthy M C and Thaddeus P 2001 *Chem. Soc. Rev.* **30** 177

[21] Ott A K, Rechtsteiner G A, Felix C, Hampe O, Jarrold M F, Van Duyne R P and Raghavachari K 1998 *J. Chem. Phys.* **109** 9652

[22] Baeyer A 1885 *Berichte der deutschen chemischen Gesellschaft* **18** 2269

[23] Tsuji M, Kuboyama S, Matsuzaki T and Tsuji T 2003 *Carbon* **41** 2141

[24] Eastmond R, Johnson T R and Walton D R M 1972 *Tetrahedron* **28** 4601

[25] Kloster-Jensen E 1972 *Angew. Chem. Int. Ed.* **11** 438

[26] Cook C L, Jones E R H and Whiting M C 1952 *J. Chem. Soc.* **546** 2883

[27] Johnson T R and Walton D R M 1972 *Tetrahedron* **28** 5221

[28] Jones E R H, Lee H H and Whiting M C 1960 *J. Chem. Soc.* **699** 3483

[29] Nakagawa M, Akiyama S, Nakasuji K and Nishimoto K 1971 *Tetrahedron* **27** 5401

[30] Lucotti A, Tommasini M, Fazzi D, Del Zoppo M, Chalifoux W A, Ferguson M J, Zerbi G and Tykwinski R R 2009 *J. Am. Chem. Soc.* **131** 4239

[31] Dembinski R, Bartik T, Bartik B, Jaeger M and Gladysz J A 2000 *J. Am. Chem. Soc.* **122** 810

[32] Antonova A B, Bruce M I, Ellis B G, Gaudio M, Humphrey P A, Jevric M, Melino G, Nicholson B K, Perkins G J, Skelton B W, Stapleton B, White A H and Zaitseva N N 2004 *Chem. Commun.* **1** 960

[33] Yam V W W, Wong K M C and Zhu N Y 2003 *Angew. Chem., Int. Ed.* **42** 1400

[34] Xu G L, Zou G, Ni Y H, DeRosa M C, Crutchley R J and Ren T 2003 *J. Am. Chem. Soc.* **125** 10057

[35] Long N J and Williams C K 2003 *Angew. Chem. Int. Ed.* **42** 2586

[36] Kastner J, Kuzmany H, Kavan L, Dousek F P and Kuerti J 1995 *Macromolecules* **28** 344

[37] Cataldo F and Capitani D 1999 *Mater. Chem. Phys.* **59** 225

[38] Cataldo F 1999 *Carbon* **37** 161

[39] Cataldo F 2004 *Polyhedron* **23** 1889

[40] Habibi A, Mousavi Khoie S M, Mahboubi F and Urgen M 2017 *Surf. Coat. Technol.* **309** 945

[41] Wu Y L, Zhang Y F, Zhu T X, Li H X, Liu Y R and Zhao X L 2019 *Chem. Phys. Lett.* **730** 64

[42] Li H R, Wu Y L, Zhang Y F, Zhu T X, Maruyama T, Liu Y and Zhao X L 2020 *Chem. Phys.* **535** 110804

[43] Peggiani S, Senis A, Facibeni A, Milani A, Serafini P, Cerrato G, Lucotti A, Tommasini M, Fazzi D, Castiglioni C, Russo V, Li Bassi A and Casari C S 2020 *Chem. Phys. Lett.* **740** 137054

[44] Shin S K, Song J K and Park S M 2011 *Appl. Surf. Sci.* **257** 5156

[45] Tsuji M, Tsuji T, Kuboyama S, Yoon S H, Korai Y, Tsujimoto T, Kubo K, Mori A and Mochida I 2002 *Chem. Phys. Lett.* **355** 101

[46] Taguchi Y, Endo H, Abe Y, Matsumoto J, Wakabayashi T, Kodama T, Achiba Y and Shiromaru H 2015 *Carbon* **94** 124

[47] Matsutani R, Inoue K, Sanada T, Wada N and Kojima K 2012 *J. Photochem. Photobiol. A* **240** 1

[48] Kucherik A O, Arakelian S M, Garnov S V, Kutrovskaya S V, Nogtev D S, Osipov A V and Khor'kov K S 2016 *Quantum Electron.* **46** 627

[49] Kucherik A, Arakelian S, Vartanyan T, Kutrovskaya S, Osipov A, Povolotskaya A, Povolotskii A and Man'shina A 2016 *Opt. Spectrosc.* **121** 263

[50] Kutrovskaya S, Chestnov I, Osipov A, Samyshkin V, Sapegina I, Kavokin A and Kucherik A 2020 *Sci. Rep.* **10** 9709

[51] Medeiros P V C, Marks S, Wynn J M, Vasylenko A, Ramasse Q M, Quigley D, Sloan J and Morris A J 2017 *ACS Nano* **11** 6178

[52] Komsa H-P, Senga R, Suenaga K and Krasheninnikov A V 2017 *Nano Lett.* **17** 3694

[53] Kobayashi K and Yasuda H 2015 *Chem. Phys. Lett.* **634** 60

[54] Senga R, Komsa H P, Liu Z, Hirose-Takai K, Krasheninnikov A V and Suenaga K 2014 *Nat. Mater.* **13** 1050

[55] Fujimori T, Morelos-Gómez A, Zhu Z, Muramatsu H, Futamura R, Urita K, Terrones M, Hayashi T, Endo M, Young Hong S, Chul Choi Y, Tománek D and Kaneko K 2013 *Nat. Commun.* **4** 2162

[56] Meunier V, Muramatsu H, Hayashi T, Kim Y A, Shimamoto D, Terrones H, Dresselhaus M S, Terrones M, Endo M and Sumpter B G 2009 *Nano Lett.* **9** 1487

[57] Ohnishi H, Kondo Y and Takayanagi K 1998 *Nature* **395** 780

[58] Hayashi T, Muramatsu H, Kim Y A, Kajitani H, Imai S, Kawakami H, Kobayashi M, Matoba T, Endo M and Dresselhaus M S 2006 *Carbon* **44** 1130

[59] Andrade N F, Vasconcelos T L, Gouvea C P, Archanjo B S, Achete C A, Kim Y A, Endo M, Fantini C, Dresselhaus M S and Souza Filho A G 2015 *Carbon* **90** 172

[60] Kim Y A, Muramatsu H, Hayashi T and Endo M 2012 *Carbon* **50** 4588

[61] Zhang Y F, Zhao J W, Fang Y H, Liu Y and Zhao X L 2018 *Nanoscale* **10** 17824

[62] Zhang Y F, Chang W W, Liu Y, Maruyama T and Zhao X L 2020 *Carbon* **158** 672

[63] Zhang J Y, Feng Y Q, Ishiwata H, Miyata Y, Kitaura R, Dahl J E P, Carlson R M K, Shinohara H and Tománek D 2012 *ACS Nano* **6** 8674

[64] Nishide D, Dohi H, Wakabayashi T, Nishibori E, Aoyagi S, Ishida M, Kikuchi S, Kitaura R, Sugai T, Sakata M and Shinohara H 2006 *Chem. Phys. Lett.* **428** 356

[65] Deng Y C and Cranford S W 2019 *Carbon* **141** 209

[66] Muramatsu H, Kim Y A, Hayashi T, Endo M, Terrones M and Dresselhaus M S 2007 *Small* **3** 788

[67] Jinno M, Ando Y, Bandow S, Fan J, Yudasaka M and Iijima S 2006 *Chem. Phys. Lett.* **418** 109

[68] Sheng L M, Jin A J, Yu L M, An K, Ando Y and Zhao X L 2012 *Mater. Lett.* **81** 222

[69] Zhao C, Kitaura R, Hara H, Irle S and Shinohara H 2011 *J. Phys. Chem. C* **115** 13166

[70] Li X, Zhang Y F, Wu Y L and Shi L 2021 *J. Appl. Phys.* **129** 064302

[71] Berd M, Puech P, Righi A, Benfdila A and Monthioux M 2012 *Small* **8** 2045

[72] Huang H, Maruyama R, Noda K, Kajiura H and Kadono K 2006 *J. Phys. Chem. B* **110** 7316

[73] Ha J H, Jung H Y, Hao J, Li B, Raeliarijaona A, Alarcón J, Terrones H, Ajayan P M, Jung Y J, Kim J and Kim D 2017 *Nanoscale* **9** 16627

[74] Shi L, Senga R, Suenaga K, Chimborazo J, Ayala P and Pichler T 2021 *Carbon* **182** 348

[75] Sanchez-Valencia J R, Dienel T, Gröning O, Shorubalko I, Mueller A, Jansen M, Amsharov K, Ruffieux P and Fasel R 2014 *Nature* **512** 61

[76] Cai J M, Ruffieux P, Jaafar R, Bieri M, Braun T, Blankenburg S, Muoth M, Seitsonen A P, Saleh M, Feng X, Müllen K and Fasel R 2010 *Nature* **466** 470

[77] Otero G, Biddau G, Sánchez-Sánchez C, Caillard R, López M F, Rogero C, Palomares F J, Cabello N, Basanta M A, Ortega J, Méndez J, Echavarren A M, Pérez R, Gómez-Lor B and Martín-Gago J A 2008 *Nature* **454** 865

[78] Sun Q, Cai L L, Wang S Y, Widmer R, Ju H, Zhu J X, Li L F, He Y B, Ruffieux P, Fasel R and Xu W 2016 *J. Am. Chem. Soc.* **138** 1106

[79] Rabia A, Tumino F, Milani A, Russo V, Bassi A L, Achilli S, Fratesi G, Onida G, Manini N, Sun Q, Xu W and Casari C S 2019 *Nanoscale* **11** 18191

[80] Kaiser K, Scriven L M, Schulz F, Gawel P, Gross L and Anderson H L 2019 *Science* **365** 1299

[81] Krasheninnikov A V and Banhart F 2007 *Nat. Mater.* **6** 723

[82] Li J X and Banhart F 2004 *Nano Lett.* **4** 1143

[83] Kis A, Csányi G, Salvetat J P, Lee T N, Couteau E, Kulik A J, Benoit W, Brugger J and Forró L 2004 *Nat. Mater.* **3** 153

[84] Terrones M, Banhart F, Grobert N, Charlier J C, Terrones H and Ajayan P M 2002 *Phys. Rev. Lett.* **89** 075505

[85] La Torre A, Romdhane F B, Baaziz W, Janowska I, Pham-Huu C, Begin-Colin S, Pourroy G and Banhart F 2014 *Carbon* **77** 906

[86] Cretu O, Botello-Mendez A R, Janowska I, Pham-Huu C, Charlier J C and Banhart F 2013 *Nano Lett.* **13** 3487

[87] La Torre A, Botello-Mendez A, Baaziz W, Charlier J C and Banhart F 2015 *Nat. Commun.* **6** 6636

[88] Liu M J, Artyukhov V I, Lee H Y, Xu F B and Yakobson B I 2013 *ACS Nano* **7** 10075

[89] Nair A K, Cranford S W and Buehler M J 2011 *Europhys. Lett.* **95** 16002

[90] Zhang Y Z, Su Y J, Wang L, Kong E S-W, Chen X S and Zhang Y F 2011 *Nanoscale Research Letters* **6** 577

[91] Liu X J, Zhang G and Zhang Y W 2015 *J. Phys. Chem. C* **119** 24156

[92] Chang C C, Hsu I K, Aykol M, Hung W H, Chen C C and Cronin S B 2010 *ACS Nano* **4** 5095

[93] Ogata S and Shibutani Y 2003 *Phys. Rev. B* **68** 165409

[94] Gao E L, Li R S and Baughman R H 2020 *ACS Nano* **14** 17071

[95] Toma S, Asaka K, Irita M and Saito Y 2019 *Surf. Interface Anal.* **51** 131

[96] Dang C Q, Chou J P, Dai B, Chou C T, Yang Y, Fan R, Lin W, Meng F L, Hu A, Zhu J, Han J, Minor A M, Li J and Lu Y 2021 *Science* **371** 76

[97] Castelli I E, Salvestrini P and Manini N 2012 *Phys. Rev. B* **85** 214110

[98] Standley B, Bao W, Zhang H, Bruck J, Lau C N and Bockrath M 2008 *Nano Lett.* **8** 3345

[99] Wang C S, Batsanov A S, Bryce M R, Martín S, Nichols R J, Higgins S J, García-Suárez V M and Lambert C J 2009 *J. Am. Chem. Soc.* **131** 15647

[100] Artyukhov V I, Liu M and Yakobson B I 2014 *Nano Lett.* **14** 4224

[101] Xu W J, Leary E, Hou S J, Sangtarash S, González M T, Rubio-Bollinger G, Wu Q, Sadeghi H, Tejerina L, Christensen K E, Agraït N, Higgins S J, Lambert C J, Nichols R J and Anderson H L 2019 *Angew. Chem., Int. Ed.* **131** 8466

[102] Scaccabarozzi A D, Milani A, Peggiani S, Pecorario S, Sun B, Tykwinski R R, Caironi M and Casari C S 2020 *J. Phys. Chem. Lett.* **11** 1970

[103] Pecorario S, Scaccabarozzi A D, Fazzi D, Gutiérrez-Fernández E, Vurro V, Maserati L, Jiang M, Losi T, Sun B, Tykwinski R R, Casari C S and Caironi M 2022 *Adv. Mater.* **34** 2110468

[104] Rode A V, Gamaly E G, Christy A G, Fitz Gerald J G, Hyde S T, Elliman R G, Luther-Davies B, Veinger A I, Androulakis J and Giapintzakis J 2004 *Phys. Rev. B* **70** 054407

[105] Levin E M, Fang X W, Bud'ko S L, Straszheim W E, McCallum R W and Schmidt-Rohr K 2008 *Phys. Rev. B* **77** 054418

[106] Ohldag H, Tyliszczak T, Höhne R, Spemann D, Esquinazi P, Ungureanu M and Butz T 2007 *Phys. Rev. Lett.* **98** 187204

[107] Ma S, Xia J H, Srikanth V V S S, Sun X, Staedler T, Jiang X, Yang F and Zhang Z D 2009 *Appl. Phys. Lett.* **95** 263105

[108] Sepioni M, Nair R R, Rablen S, Narayanan J, Tuna F, Winpenny R, Geim A K and Grigorieva I V 2010 *Phys. Rev. Lett.* **105** 207205

[109] Chen J W, Yang L F, Yang H T and Dong J M 2003 *Phys. Lett. A* **316** 101

[110] Zanolli Z, Onida G and Charlier J C 2010 *ACS Nano* **4** 5174

[111] Yang F, Liu P, Wu C W, Yao D X and Yang G W 2021 *Mater. Today Commun.* **26** 102152

[112] Chalifoux W A and Tykwinski R R 2010 *Nat. Chem.* **2** 967

[113] Qin J X, Yang X G, Shen C L, Chang Y, Deng Y, Zhang Z F, Liu H, Lv C F, Li Y Z, Zhang C, Dong L and Shan C X 2022 *Nano Energy* **101** 107549

[114] Peggiani S, Marabotti P, Lotti R A, Facibeni A, Serafini P, Milani A, Russo V, Bassi A L and Casari C S 2020 *Phys. Chem. Chem. Phys.* **22** 26312

[115] Gibtner T, Hampel F, Gisselbrecht J-P and Hirsch A 2002 *Chem. - Eur. J.* **8** 408

[116] Mostaani E, Monserrat B, Drummond N D and Lambert C J 2016 *Phys. Chem. Chem. Phys.* **18** 14810

[117] Eisler S, Slepkov A D, Elliott E, Luu T, McDonald R, Hegmann F A and Tykwinski R R 2005 *J. Am. Chem. Soc.* **127** 2666

[118] Zheng Q L and Gladysz J A 2005 *J. Am. Chem. Soc.* **127** 10508

[119] Tabata H, Fujii M, Hayashi S, Doi T and Wakabayashi T 2006 *Carbon* **44** 3168

[120] Zheng Q L, Bohling J C, Peters T B, Frisch A C, Hampel F and Gladysz J A 2006 *Chem. - Eur. J.* **12** 6486

[121] Shi L, Senga R, Suenaga K, Kataura H, Saito T, Paz A P, Rubio A, Ayala P and Pichler T 2021 *Nano Lett.* **21** 1096

[122] Mohr W, Stahl J, Hampel F and Gladysz J A 2003 *Chem. - Eur. J.* **9** 3324

[123] Zirzlmeier J, Schrettl S, Brauer J C, Contal E, Vannay L, Brémond é, Jahnke E, Guldi D M, Corminboeuf C, Tykwinski R R and Frauenrath H 2020 *Nat. Commun.* **11** 4797

[124] Rohringer P, Shi L, Liu X, Yanagi K and Pichler T 2014 *Carbon* **74** 282

[125] Rohringer P, Shi L, Ayala P and Pichler T 2016 *Adv. Funct. Mater.* **26** 4874

[126] Shi L, Yanagi K, Cao K, Kaiser U, Ayala P and Pichler T 2018 *ACS Nano* **12** 8477

[127] Xiao J, Li J L and Yang G W 2017 *Small* **13** 1603495

[128] Kutrovskaya S, Osipov A, Baryshev S, Zasedatelev A, Samyshkin V, Demirchyan S, Pulci O, Grassano D, Gontrani L, Hartmann R R, Portnoi M E, Kucherik A, Lagoudakis P G and Kavokin A 2020 *Nano Lett.* **20** 6502

[129] Kutrovskaya S, Demirchyan S, Osipov A, Baryshev S, Zasedatelev A, Lagoudakis P and Kavokin A 2021 *Phys. Rev. Research* **3** 013071

[130] Tschannen C D, Gordeev G, Reich S, Shi L, Pichler T, Frimmer M, Novotny L and Heeg S 2020 *Nano Lett.* **20** 6750

[131] Qin J X, Yang X G, Lv C F, Li Y Z, Liu K K, Zang J H, Yang X, Dong L and Shan C X 2021 *Materials & Design* **210** 110091

[132] Fantini C, Cruz E, Jorio A, Terrones M, Terrones H, Van Lier G, Charlier J C, Dresselhaus M S, Saito R, Kim Y A, Hayashi T, Muramatsu H, Endo M and Pimenta M A 2006 *Phys. Rev. B* **73** 193408

[133] Wanko M, Cahangirov S, Shi L, Rohringer P, Lapin Z J, Novotny L, Ayala P, Pichler T and Rubio A 2016 *Phys. Rev. B* **94** 195422

[134] Shi L, Rohringer P, Wanko M, Rubio A, Waßerroth S, Reich S, Cambré S, Wenseleers W, Ayala P and Pichler T 2017 *Phys. Rev. Materials* **1** 075601

[135] Yang X G, Lv C F, Yao Z, Yao M G, Qin J X, Li X, Shi L, Du M R, Liu B B and Shan C X 2020 *Carbon* **159** 266

[136] Endo M, Kim Y A, Hayashi T, Muramatsu H, Terrones M, Saito R, Villalpando-Paez F, Chou S G and Dresselhaus M S 2006 *Small* **2** 1031

[137] Agarwal N R, Lucotti A, Fazzi D, Tommasini M, Castiglioni C, Chalifoux W a. and Tykwinski R R 2013 *J. Raman Spectrosc.* **44** 1398

[138] Eastmond R and Walton D R M 1972 *Tetrahedron* **28** 4591

[139] Martinati M, Wenseleers W, Shi L, Pratik S M, Rohringer P, Cui W, Pichler T, Coropceanu V, Brédas J L and Cambré S 2022 *Carbon* **189** 276

[140] Rayleigh 1896 *Science* **42** 167

[141] Abbe E 1873 *Archiv f. mikrosk. Anatomie* **9** 413

[142] Tschannen C D, Frimmer M, Gordeev G, Vasconcelos T L, Shi L, Pichler T, Reich S, Heeg S and Novotny L 2021 *ACS Nano* **15** 12249

[143] Timoshevskii A, Kotrechko S and Matviychuk Yu 2015 *Phys. Rev. B* **91** 245434

[144] Hu Y H 2011 *J. Phys. Chem. C* **115** 1843

[145] Cahangirov S, Topsakal M and Ciraci S 2010 *Phys. Rev. B* **82** 195444

[146] Hu Y H 2009 *Phys. Lett. A* **373** 3554

[147] Luo W Q and Windl W 2009 *Carbon* **47** 367

[148] Wong C H, Buntov E A, Rychkov V N, Guseva M B and Zatsepin A F 2017 *Carbon* **114** 106

[149] Yang X M, Huang Y H, Cao B Y and To A C 2017 *Physica E* **93** 124

[150] Lin Y C, Morishita S, Koshino M, Yeh C H, Teng P Y, Chiu P W, Sawada H and Suenaga K 2017 *Nano Lett.* **17** 494

[151] Shang Y C, Shen F R, Hou X Y, Chen L Y, Hu K, Li X, Liu R, Tao Q, Zhu P W, Liu Z D, Yao M G, Zhou Q, Cui T and Liu B B 2020 *Chin. Phys. Lett.* **37** 080701

[152] Lou Q, Yang X G, Liu K K, Ding Z Z, Qin J X, Li Y Z, Lv C F, Shang Y, Zhang Y W, Zhang Z F, Zang J H, Dong L and Shan C X 2022 *Nano Res.* **15** 2545

[153] Yang X G, Dong J J, Yao M G, Hu K, Sun H H, Liu R, Shan C X and Liu B B 2021 *Carbon* **172** 13

[154] Shang Y C, Liu Z D, Dong J J, Yao M G, Yang Z X, Li Q J, Zhai C G, Shen F R, Hou X Y, Wang L, Zhang N Q, Zhang W, Fu R, Ji J F, Zhang X M, Lin H, Fei Y W, Sundqvist B, Wang W H and Liu B B 2021 *Nature* **599** 599

[155] Yang X G, Lv C, Liu S J, Zang J H, Qin J X, Du M R, Yang D W, Li X, Liu B B and Shan C X 2020 *Carbon* **156** 309

[156] Yang X G, Yao M G, Wu X Y, Liu S J, Chen S L, Yang K, Liu R, Cui T, Sundqvist B and Liu B B 2017 *Phys. Rev. Lett.* **118** 245701

[157] Wang L, Liu B B, Li H, Yang W G, Ding Y, Sinogeikin S V, Meng Y, Liu Z X, Zeng X C and Mao W L 2012 *Science* **337** 825

[158] Andrade N F, Aguiar A L, Kim Y A, Endo M, Freire P T C, Brunetto G, Galvão D S, Dresselhaus M S and Souza Filho A G 2015 *J. Phys. Chem. C* **119** 10669

[159] Neves W Q, Alencar R S, Ferreira R S, Torres-Dias A C, Andrade N F, San-Miguel A, Kim Y A, Endo M, Kim D W, Muramatsu H, Aguiar A L and Souza Filho A G 2018 *Carbon* **133** 446
[160] Neves W Q, Ferreira R S, Kim Y A, Endo M, Choi G B, Muramatsu H, Aguiar A L, Alencar R S and Souza Filho A G 2022 *Carbon* **196** 20
[161] Sharma K, Costa N L, Kim Y A, Muramatsu H, Barbosa Neto N M, Martins L G P, Kong J, Paschoal A R and Araujo P T 2020 *Phys. Rev. Lett.* **125** 105501
[162] Faria B, Silvestre N, Bernardes C and Lopes J N C 2020 *Physica E* **117** 113831
[163] Ravagnan L, Manini N, Cinquanta E, Onida G, Sangalli D, Motta C, Devetta M, Bordoni A, Piseri P and Milani P 2009 *Phys. Rev. Lett.* **102** 245502
[164] Xu D G, Hou L, Dong J S, Hu H M and Ouyang G 2021 *Phys. Status Solidi RRL* **15** 2100390
[165] Hu F, Zeng C, Long R, Miao Y, Wei L, Xu Q and Min W 2018 *Nat. Methods* **15** 194
[166] Rusznyák á, Zólyomi V, Kürti J, Yang S and Kertesz M 2005 *Phys. Rev. B* **72** 155420
[167] Tapia A, Aguilera L, Cab C, Medina-Esquivel R A, de Coss R and Canto G 2010 *Carbon* **48** 4057
[168] Moura L G, Malard L M, Carneiro M A, Venezuela P, Capaz R B, Nishide D, Achiba Y, Shinohara H and Pimenta M A 2009 *Phys. Rev. B* **80** 161401
[169] Hu Z L, Guo X M and Ru C Q 2008 *Nanotechnology* **19** 305703
[170] Wang Y, Huang Y H, Yang B H and Liu R Z 2008 *Carbon* **46** 276
[171] Heeg S, Shi L, Poulikakos L V, Pichler T and Novotny L 2018 *Nano Lett.* **18** 5426